



AMERICAN METEOROLOGICAL SOCIETY

Bulletin of the American Meteorological Society

EARLY ONLINE RELEASE

This is a preliminary PDF of the author-produced manuscript that has been peer-reviewed and accepted for publication. Since it is being posted so soon after acceptance, it has not yet been copyedited, formatted, or processed by AMS Publications. This preliminary version of the manuscript may be downloaded, distributed, and cited, but please be aware that there will be visual differences and possibly some content differences between this version and the final published version.

The DOI for this manuscript is doi: 10.1175/BAMS-D-16-0009.1

The final published version of this manuscript will replace the preliminary version at the above DOI once it is available.

If you would like to cite this EOR in a separate work, please use the following full citation:

L'Heureux, M., K. Takahashi, A. Watkins, A. Barnston, E. Becker, T. Di Liberto, F. Gamble, J. Gottschalck, M. Halpert, B. Huang, K. Mosquera-Vásquez, and A. Wittenberg, 2016: Observing and Predicting the 2015-16 El Niño. *Bull. Amer. Meteor. Soc.* doi:10.1175/BAMS-D-16-0009.1, in press.



Observing and Predicting the 2015-16 El Niño

Michelle L. L'Heureux*

*National Oceanic and Atmospheric Administration,
NWS/NCEP/Climate Prediction Center, College Park, MD, USA*

Ken Takahashi

Instituto Geofísico del Perú, Lima, Peru

Andrew B. Watkins

Australian Bureau of Meteorology, Melbourne, Australia

Anthony G. Barnston

*International Research Institute for Climate and Society,
Columbia University, New York, NY, USA*

Emily J. Becker

NOAA Climate Prediction Center/Innovim, College Park, MD, USA

Tom E. Di Liberto

NOAA Climate Prediction Center/Innovim, College Park, MD, USA

Felicity Gamble

Australian Bureau of Meteorology, Melbourne, Australia

Jon Gottschalck

NOAA Climate Prediction Center, College Park, MD, USA

Michael S. Halpert

NOAA Climate Prediction Center, College Park, MD, USA

Boyin Huang

NOAA National Centers for Environmental Information, Asheville, NC, USA

Kobi Mosquera-Vásquez

Instituto Geofísico del Perú, Lima, Peru

Andrew T. Wittenberg

NOAA Geophysical Fluid Dynamics Laboratory, Princeton, NJ, USA

*Corresponding author address: National Oceanic and Atmospheric Administration,
NWS/NCEP/Climate Prediction Center, 5830 University Research Ct, College Park, MD
20740, USA

E-mail: michelle.lheureux@noaa.gov

ABSTRACT

32 The El Niño of 2015-16 was among the strongest El Niño events observed
33 since 1950, and took place almost two decades after the previous major event
34 in 1997-98. Here, perspectives of the event are shared by scientists from
35 three national meteorological or climate services that issue regular opera-
36 tional updates on the status and prediction of the El Niño-Southern Oscil-
37 lation (ENSO). Public advisories on the unfolding El Niño were issued in the
38 first half of 2015. This was followed by significant growth in sea surface
39 temperature (SST) anomalies, a peak during November 2015 - January 2016,
40 subsequent decay, and its demise during May 2016. The lifecycle and mag-
41 nitude of the 2015-16 El Niño was well predicted by most models used by
42 national meteorological services, in contrast to the generally over-exuberant
43 model predictions made the previous year. The evolution of multiple atmo-
44 spheric and oceanic measures demonstrates the rich complexity of ENSO, as
45 a coupled ocean-atmosphere phenomenon with pronounced global impacts.
46 While some aspects of the 2015-16 El Niño rivaled the events of 1982-83 and
47 1997-98, we show that it also differed in unique and important ways, with im-
48 plications for the study and evaluation of past and future ENSO events. Unlike
49 previous major El Niños, remarkably above-average SST anomalies occurred
50 in the western and central equatorial Pacific, but were milder near the coast of
51 South America. While operational ENSO systems have progressed markedly
52 over the past several decades, the 2015-16 El Niño highlights several chal-
53 lenges that will continue to test both the research and operational forecast
54 communities.

55 CAPSULE SUMMARY: The El Niño of 2015-16 rivaled the major El Niño events of 1982-83
56 and 1997-98, showcasing advancements in operational observing and prediction systems, while
57 offering challenges for the future.

58 **1. Introduction**

59 The 2015-16 El Niño was likely the most widely anticipated El Niño-Southern Oscillation
60 (ENSO) event ever, and it was preceded by nearly four decades of advancements in observing
61 and prediction systems. Unlike the previous major El Niño event of 1997-98 (e.g., McPhaden
62 1999), the most recent El Niño was embedded within the fabric of the Internet and social media,
63 with arguably more frequent updates and pathways to convey information than ever before. By
64 mid-2015, operational forecast centers around the world were nearly unanimous: El Niño was
65 very likely to be strong, with the potential of rivaling previous major El Niño events in 1982-83
66 and 1997-98. Given the widespread coverage of these ENSO outlooks and the comparisons made
67 to other similarly strong El Niño events, there was considerable concern about significant global
68 impacts. While the El Niño phenomenon itself was well predicted in 2015-16, climate impacts
69 near El Niño's peak matched historical patterns in some areas (e.g., Ropelewski and Halpert 1987;
70 Halpert and Ropelewski 1992), but in other regions, additional climate factors clearly played a
71 role.

72 Because the ENSO cycle, with its warm (El Niño) and cool (La Niña) phases, is a leading source
73 of seasonal climate variability and predictability, it is closely monitored by many national and in-
74 ternational organizations. The authorship on this paper is composed of individuals associated with
75 three national-level assessments on ENSO from the National Oceanic and Atmospheric Adminis-
76 tration (NOAA) in the United States, the Bureau of Meteorology (BoM) in Australia, and one of
77 the agencies that comprises the Multisectoral Committee of the National Study of El Niño (EN-

78 FEN) in Peru. All provide operational, or regularly updated, ENSO assessments, in part because
79 these countries are known to have climates — and indeed economies and societies — significantly
80 influenced by ENSO. These three agencies also happen to be geographically complementary, span-
81 ning the Pacific Ocean basin. They go beyond the automatic generation of observational and model
82 output to provide summary level information of the progress of ENSO and its forecast, which is
83 aimed at a diverse set of users among the general public, whose knowledge ranges from technically
84 savvy to novice.

85 ENSO is a sprawling and multi-faceted coupled ocean-atmosphere climate phenomenon that
86 affects every country in a different manner. Table 1 summarizes the current El Niño definitions and
87 watch/alert/warning systems in association with the national-level ENSO updates. As in past years,
88 the timing of El Niño status updates and declarations varied during 2015-16 due to differences in
89 datasets and ENSO criteria and thresholds, which are governed by differing regional impacts. For
90 example, Peru issues forecasts for a “coastal El Niño” because the amount of coastal rainfall they
91 receive is very sensitive to how warm sea surface temperatures (SST) adjacent to South America
92 become (e.g., Takahashi 2004). Ultimately, though, every agency examines a broad range of
93 oceanic and atmospheric anomalies to inform their updates. Internationally, the Niño-3.4 SST
94 region (thin red box in Fig. 6, in the east-central equatorial Pacific Ocean, is perhaps the most
95 common measure of ENSO because this region is strongly coupled with the overlying atmosphere
96 (e.g., Barnston et al. 1997) and to global teleconnections. This index also tends to be the focus of
97 operational model displays.

98 These operational updates have evolved over past decades due to lessons learned from previous
99 ENSO events and user demands placed on them. The 2015-16 El Niño not only showcased the
100 latest generation of ENSO climate services, but this knowledge was disseminated and interpreted
101 across a wide variety of media platforms, ranging from traditional mainstream outlets to social

102 media — a vastly different communication environment compared to the last major El Niño event
103 of 1997-98. This came with its own set of advantages, such as exposure to far broader audiences,
104 and disadvantages, such as the sometimes-questionable interpretation of datasets and forecast out-
105 looks, which differed from official assessments. While the ENSO assessments and dissemination
106 processes vary by national agency, the following sections summarize our collective experience in
107 tracking the observational evolution, verifying the model forecasts, and documenting the global
108 climate anomalies associated with the historic 2015-16 El Niño.

109 **2. Datasets and Methods**

110 Since the major El Niño of 1997-98, many observational reconstructions and reanalysis datasets
111 have been created or improved. Unlike station-based data or point “in situ” observations (e.g. a
112 buoy), these gridded datasets are complete both spatially and temporally and, for the statistical
113 reconstructions of SST, extend as far back as the late 1800s. Several operationally oriented centers
114 update datasets in near real-time, which allows scientists to monitor the tropical Pacific. Given
115 the interest in the 2015-16 El Niño and its potential impacts, these real-time datasets were popular
116 with users, many of whom were interested in the strength of the event and its ranking relative to
117 past El Niño events.

118 Complicating this assessment, however, each center relies on a set of core observational datasets
119 for its ENSO updates, so the exact values for a given variable (e.g. Niño-3.4 SST) will vary de-
120 pending which dataset is examined. These differences between datasets primarily arise due to
121 structural reasons, such as the choice of the dynamical model or the statistical method used to
122 infill between available observations. The disparities are particularly evident across the tropical
123 Pacific Ocean, which contains large regions that are not covered by point measurements (e.g.
124 buoys, ships). Many centers additionally rely on datasets that ingest not only buoy or ship data,

125 but also satellite information. However, the modern satellite record began in the late 1970s, which
126 prevents the use of these datasets for historical rankings going further back in time. Moreover,
127 satellite estimates have biases (due to issues like varying equatorial crossing times), which need to
128 be corrected by in situ surface observations, and these corrections can vary over time and space as
129 new satellites are incorporated (e.g., Huang et al. 2015a). Some datasets like the NOAA Extended
130 Reconstructed SST (ERSST) opt to not include satellite information in order to preserve the con-
131 sistency, or homogeneity, of the record. But, for purposes outside of historical comparisons and
132 to provide more real-time ENSO updates, these satellite-based datasets are strongly relied upon
133 both to get an overall sense of the ENSO evolution and as the initial conditions for many forecast
134 models.

135 Because of the interest in how the 2015-16 event compares with other major El Niño events, we
136 prioritize datasets that are routinely updated and, when possible, datasets that were constructed
137 with the intent of providing a consistent, homogenous climate record. Individually, none of these
138 datasets represent “the truth” or perfect measurements over the entire tropical Pacific Ocean. For
139 that reason, in addition to showing the individual datasets, we also display the average of multiple
140 datasets to compare events, which we hypothesize can reduce the structural error associated with
141 the observational datasets, analogous to the reduction of error through multi-model averaging (e.g.,
142 DelSole et al. 2014).

143 To compare historical strength, we focus on the SST statistical reconstructions: two versions of
144 ERSST (v3b and v4; Smith et al. 2008; Huang et al. 2015b), the Hadley Centre SST (HadISST;
145 Rayner et al. 2003), and the Centennial In Situ Observation-Based Estimates (COBE) SST (Ishii
146 et al. 2005), which extend back to the late 1800s. All Niño index regions (shown in Fig. 6)
147 are computed to provide a sense of how the events varied in location. These indices span the
148 equatorial Pacific Ocean and are used to summarize the breadth of the SST anomalies and where

149 they are largest. Thus, these regions are also used to provide information on the “El Niño flavor,”
150 a term popularized in recent years to describe the continuum of different spatial patterns of SST
151 anomalies that result from ENSO (Capotondi et al. 2015).

152 To evaluate the tropical Pacific atmosphere, we feature the zonal gradient of 1000-hPa geopo-
153 tential height between Indonesia and the eastern equatorial Pacific, the Equatorial Southern Os-
154 cillation Index (EQSOI) and the more traditional, station-based Tahiti minus Darwin Southern
155 Oscillation Index (SOI). To compare the former, we use seven reanalysis datasets that extend back
156 to at least 1979 (see caption of Fig. 5). We also examine three satellite-based outgoing longwave
157 radiation (OLR) records, a proxy for tropical convection, which compared to precipitation, is bet-
158 ter monitored over the tropical Pacific Ocean and therefore more stable in time and space. Data are
159 based on the Advanced Very High Resolution Radiometer (AVHRR; Liebmann and Smith 1996)
160 and the High Resolution Infrared Radiation Sounder (HIRS) v2r2 and v2r7 (Lee et al. 2007).

161 To describe the within event evolution of the 2015-16 El Niño and how similar it was to past
162 major events, we make use of the daily depth of the 20°C isotherm from the Tropical Atmo-
163 sphere Ocean (TAO; McPhaden et al. 2010) buoys and Argo floats (e.g., Roemmich and Gilson
164 2009), weekly SST from Optimal Interpolation SST (OISSTv2; Reynolds et al. 2002), and daily
165 10-meter winds from ERA-Interim (Dee et al. 2011). To evaluate the combined multi-model fore-
166 casts made by the IRI and Climate Prediction Center (CPC) during 2014-16, the newer, higher
167 resolution (0.25°x0.25°) daily OISST product is used to compute seasonal mean Niño-3.4 index
168 values (Reynolds et al. 2007). While most models are not initialized with the same SST data, the
169 dynamical models use higher resolution analyses like the daily OISST.

170 To examine the 500-hPa geopotential height anomalies over the globe during the Northern
171 Hemisphere winter, we make use of monthly data from the NCEP/NCAR Reanalysis (Kalnay
172 et al. 1996). Observed surface air temperature data are obtained from the 2.5°x2.5° gridded

173 GHCN+CAMS temperature dataset (Fan and van den Dool 2008), a combination of two large
174 station datasets, the Global Historical Climate Network (GHCN) and Climate Anomaly Moni-
175 toring System (CAMS). Global precipitation data are from the 2.5°x2.5° gridded Precipitation
176 Reconstruction Dataset (PREC; Chen et al. 2002), which is also based on gauge observations from
177 GHCN and CAMS.

178 Unless clearly specified otherwise, anomalies are calculated as departures from a 1981-2010
179 monthly mean climatology or, for sub-monthly data, a climatology that is based on the first four
180 harmonics of the seasonal cycle. Because of this fixed 30-year base period, longer decadal or
181 secular trends are likely to be incorporated into the anomalies (e.g., L'Heureux et al. 2013).

182 **3. Evolution of Tropical Pacific Oceanic and Atmospheric Anomalies**

183 During the 2015-16 El Niño, all of the Niño SST indices registered values that were at least
184 among the top three in the historical record, reinforcing its categorization as one of the strongest
185 El Niño events on record extending at least back to 1950. Fig. 1 presents the evolution of the
186 seasonal (3-month) average values of the Niño SST indices during 2015-16 relative to 1972-73,
187 1982-83, and 1997-98. Overlapping seasonal index values are presented because ENSO is a cli-
188 mate phenomenon, typically identified on seasonal-to-interannual timescales. With the exception
189 of Niño-1+2, the Niño indices were nearly +0.5°C above average at the beginning of 2015. This
190 was warmer than at the start of 1997 and 1982 and likely the remnants of a borderline El Niño-
191 Neutral situation in 2014 (McPhaden 2015). Positive SST anomalies were largest near the In-
192 ternational Date Line through March 2015 (Fig. 2, left panel). Beneath the surface, temperature
193 anomalies were also warm in the western and central equatorial Pacific (Fig. 3, left panel). As in
194 1997, a series of westerly wind bursts during the first quarter of 2015 (Fig. 4, left panel) resulted in
195 the eastward progression of a downwelling oceanic Kelvin wave (Fig. 3, left panel). As the ther-

196 mocline deepened in the eastern Pacific, positive SST anomalies significantly strengthened near
197 South America where the Niño-1+2 and Niño-3 indices reached $+1.5^{\circ}\text{C}$ by May-June-July (MJJ)
198 2015 (Fig. 1, bottom row).

199 The region of the largest positive SST anomalies expanded westward from May through Novem-
200 ber 2015, which was also similar to the evolution during 1997 (Fig. 2). Primarily because of the
201 increase of the thermocline depth and surface temperatures anomalies, NOAA, BoM, and ENFEN
202 all declared the onset of El Niño conditions by mid-May 2015. Most Niño regions closely tracked
203 the evolution of the 1997-98 El Niño through July 2015, which, alongside model forecasts, was
204 factored into the outlooks as corroborating information that this event would likely peak as a strong
205 event based on warming in the Niño 3.4 and the Niño 1+2 indices. In accordance with this out-
206 look, the Niño-3.4 and Niño-3 indices grew monotonically during the rest of 2015, peaking near
207 $+2.5^{\circ}\text{C}$ during November-December-January (NDJ) 2015-16 (Fig. 1). However, across the eastern
208 Pacific, the thermocline depth anomalies during NDJ 2015-16 were not as deep as 1997-98.

209 Going back to at least 1950, seasonal Niño-3.4 index values were near record at the peak of
210 the event, but the spread among different datasets (Fig. 1) and the uncertainty as documented in
211 ERSSTv4 by Huang et al. (2016) precludes clear designation as a record. The westernmost Niño-4
212 index values were particularly remarkable compared to the previous events, with seasonal values
213 near $+1.0^{\circ}\text{C}$ through most of 2015, and a peak just shy of 1.5°C during NDJ 2015-16. In contrast,
214 the other significant El Niño events failed to reach $+1^{\circ}\text{C}$. Interestingly, the 2015-16 warming in
215 the Niño-4 region was comparable to that of the 2009-10 El Niño, which was not a major event,
216 but had record warming in this region (Lee and McPhaden 2010).

217 After the midpoint of 2015, the growth in the Niño 1+2 and Niño-3 SST indices noticeably
218 slowed relative to the 1997-98 El Niño (Fig. 1). In fact, the easternmost Niño-1+2 index did not
219 perceptibly strengthen beyond the May-June-July 2015 (MJJ) value of $+2^{\circ}\text{C}$, which clearly fell

220 short of the nearly +4°C maximum achieved during the 1997-98 and 1982-83 events. While there
221 were roughly the same number of downwelling Kelvin waves as in 1997-98, they did not have
222 as much of an influence on the amplitude of the subsurface temperature anomalies in the eastern
223 Pacific (Fig. 3), consistent with the smaller eastward extent, and weaker magnitude, of the westerly
224 wind anomalies (Fig. 4). This may be tied to cooling related to the decadal shift toward stronger
225 trade winds (e.g., Hu et al. 2013) or possibly related to the non-linear convective feedback across
226 the eastern Pacific Ocean (e.g., Takahashi and Dewitte 2016).

227 Indices that measure the atmospheric component of ENSO over the tropical Pacific (e.g. pressure
228 and convection) were also indicative of an impressive El Niño in 2015-16, albeit not record-setting.
229 Fig. 5 (top panel) shows that the traditional Southern Oscillation Index (SOI), based on the differ-
230 ence in sea level pressure between Tahiti minus Darwin stations (dashed lines), and the Equatorial
231 SOI (solid lines) were both substantially negative, reflecting the weakening of the Pacific Walker
232 circulation that is typical of El Niño. During 2015-16, the SOI minimum was nearly 2 standard
233 deviations below the 1981-2010 mean, and the minimum EQSOI value was approximately -2.5
234 standard deviations using the mean of the reanalyses, with noticeable spread among the individual
235 datasets. The 2015-16 values were not as low as in 1982-83 (the historical record for both the SOI
236 and EQSOI) and also fell short of 1997-98 values.

237 The OLR indices over the eastern and central tropical Pacific Ocean were also quite negative,
238 indicating increased convection and rainfall over the areas of above-average SST (Fig. 5, middle
239 and bottom panels; Chiodi and Harrison 2013; L'Heureux et al. 2015). The eastern Pacific OLR
240 index is strongly skewed compared to the central Pacific index, reflecting non-linearity in SSTs
241 (e.g., Takahashi and Dewitte 2016), so the differences in evolution with 1997-98 and 1982-83 are
242 more dramatic. However, seasonal values in both indices were among the top three most significant
243 events.

244 As is typical with the evolution of ENSO events, all ENSO indices weakened after the Northern
245 Hemisphere winter of 2015-16. As the event decayed, there was a steeper drop off in the eastern
246 regions of Niño-1+2 and Niño-3 compared to 1982-83 and in Niño-1+2 compared to 1997-98 (Fig.
247 1). The Niño-1+2 region was most similar to the trajectory of 1972-73, which was in stark contrast
248 to the 1982-83 event that maximized during May-June-July of the second year and the 1997-98
249 event. During the latter two events, the anomalous westerly winds across the eastern Pacific helped
250 to maintain larger positive SST anomalies (Vecchi and Harrison 2006), which were absent in 2015-
251 16 (Fig. 4). After April-May-June (AMJ) 2016, the Niño regions returned to values reflective of
252 ENSO-neutral conditions, though the decrease in Niño-4 lagged the other El Niño events because
253 it achieved higher SST anomalies at its peak.

254 Overall, one of the more distinct aspects of 2015-16 El Niño, compared to 1997-98 and 1982-
255 83, was the cooler SST anomalies in the east and warmer SST anomalies in the west; this was
256 especially noticeable at the maximum in November and December 2015 (Fig. 2). Consistent with
257 the Bjerknes feedback (coupling between SST and wind anomalies), Fig. 4 shows that the westerly
258 wind anomalies from August through December 2015 were not as strong as in the same months
259 in 1997 over the central and eastern equatorial Pacific Ocean (this is also replicated using NCEP
260 CFSR 10-m winds; not shown). Hence, relative to the *anomalies* of the last major El Niño, the
261 zonal or east-west differences in anomalous SST, subsurface temperatures, winds, and pressure
262 during the last half of 2015 were not as pronounced across the equatorial Pacific Ocean.

263 Supp. Figs. 1 and 2 also indicate that the anomalous meridional SST gradient was more relaxed
264 during 2015-16 relative to 1997-98 and 1982-83. Typically, during El Niño, SSTs are above
265 average on the equator and then taper to smaller values off the equator. During 2015-16, across
266 the eastern Pacific (150°W-90°W), the anomalous SSTs were relatively warmer just to the north of
267 the equator (5°-10°N) and cooler immediately on the equator (2.5°S-2.5°N). Supp. Fig. 2 suggests

268 that the weakening of the typical anomalous El Niño meridional gradient was associated with a
269 corresponding dearth of enhanced convection across the central and eastern Pacific Ocean (also
270 see Fig. 5).

271 The exceptional Niño-4 SST index values reflect the enhanced westward extension of positive
272 SST anomalies during 2015-16. While one could define this pattern as a major El Niño event with
273 a bit of a “Central Pacific” flavor in a relative sense compared to the other major events, it would
274 be remiss not to point out the broad stretch of above-average SSTs extending across the central
275 and eastern equatorial Pacific. In fact, the SST anomalies with the largest amplitudes occurred
276 within the east-central Pacific and, in particular, within the Niño-3.4 region (Fig. 1). Fig. 6 shows
277 that the observed SST anomalies spatially correlate very well onto the pattern that results from
278 regressing SST anomalies onto the Niño-3.4 index. At its peak in November-January, the pattern
279 of SST anomalies extended farther westward and projected better onto the Niño-3.4 index than in
280 previous major El Niño events (Supp. Fig. 1).

281 In addition to the most recent El Niño projecting well onto the Niño-3.4 index relative to past
282 years between 1982-2016 (compare individual black dots in bottom panels of Fig. 6), the 2015-
283 16 boreal winter also was associated with nearly equal weights (~ 2 standard deviation values)
284 in the so-called “E” and “C” indices of Takahashi et al. (2011). While there are many different
285 indices to evaluate ENSO flavors, the “E” and “C” indices isolate SST anomalies in the eastern and
286 central equatorial Pacific Ocean, respectively. For example, the 1982-83 and 1997-98 El Niño had
287 strongly projected onto the “E” index relative to 2015-16, while the previous El Niño in 2009-10
288 was well captured by the “C” index. Therefore, the most recent event was approximately in the
289 middle of the ENSO continuum (Capotondi et al. 2015), with less intensification in the far eastern
290 Pacific Ocean.

291 **4. Model Forecasts of the Niño-3.4 Sea Surface Temperature Index**

292 Operational forecast centers consider their own in-house climate models and a number of model
293 plumes, which display members and/or ensemble means from an assortment of different models.
294 The IRI/CPC multi-model plume of Niño 3.4 SST forecasts is perhaps the longest running, opera-
295 tional collection of various models, which includes both dynamical and statistical models. Once a
296 month, agencies around the world provide ensemble-average, overlapping seasonal Niño-3.4 SST
297 index values going out to 9 months. The exact dates of initialization, number of members in the
298 ensemble mean, and mean bias correction is left up to the model providers.

299 An average of the multi-model ensemble (MME) of just over 15 “dynamical” and nearly 10
300 “statistical” models are displayed in the latest updates of the IRI/CPC plume¹. However, embedded
301 within the dynamical category are a set of ~ 5 models called Intermediate-complexity Coupled
302 Models (ICMs) that are not comprehensive like the state-of-the-art dynamical models and rely
303 more heavily on statistical methods. Over the last couple of years, in general, the skill scores
304 associated with the dynamical average improves when the ICM are excluded, and the ICM-only
305 average is not an improvement upon the statistical model average (Supplementary Figs. 3-5).

306 Fig. 7 illustrates, in grey-scale, every individual model forecast made for targets during DJF
307 2013-14 through FMA 2015-16 for the dynamical (top panel), which include the ICMs, and sta-
308 tistical models (bottom panel). The solid blue and red lines lie within the spread of the grey lines
309 because they represent the MME average of the individual models. Generally, the MME mean
310 tends to be more skillful than any individual model because the averaging helps to cancel out
311 model error (Palmer et al. 2004; Kirtman et al. 2014). However, a single observation will be a
312 result of some predictable signal (e.g. ENSO dynamics) and unpredictable, random noise, while

¹Dynamical models typically require supercomputing resources, involve data assimilation systems, and explicitly calculate the future state based on the physics of the atmosphere, land, ice and oceans and their interactions. Statistical models can be run on a desktop computer, and rely upon historical relationships in the observational record and assumes these relationships will hold into the future.

313 averaging in the MME is designed to suppress the unpredictable noise in order to enhance the
314 signal. ENSO events are forecast opportunities when the role of the predictable signal becomes
315 greater than the typical level of noise (e.g., Vecchi et al. 2006; Kumar and Hu 2014).

316 The 2015-16 predictions of the Niño-3.4 SST index were successful, especially when juxtaposed
317 with the low ENSO predictability of the previous decade (Barnston et al. 2012) and the predictions
318 of an El Niño in 2014-15 that did not grow as expected (McPhaden 2015). For target periods in
319 2014, the statistical MME average anomalies (blue lines) were closer to the observed anomalies
320 (black line), while the dynamical MME average (red lines) largely over-forecasted the amount of
321 warming in Niño-3.4. But, after mid-2014, the forecasts improved and were generally closer to
322 the modest warming (Niño-3.4 near $+0.5^{\circ}\text{C}$) observed for several seasons in 2014-15.

323 Coming out of the 2014-15 Northern Hemisphere winter, a number of dynamical and statistical
324 models were predicting a decrease in the Niño 3.4 index. Once the observational data showed
325 warming in early 2015, many dynamical and statistical models began to forecast a more significant
326 El Niño. However, both MME averages underestimated the peak strength of the episode, not
327 catching onto the possibility of a $+2^{\circ}\text{C}$ sized event until mid-July 2015 for the dynamical and
328 mid-August 2015 for the statistical.

329 By August 2015, official ENSO outlooks were more assertively playing up the potential of a
330 historically strong event. At this time, public communications explicitly favored an event rivaling
331 the peak amplitudes of past major El Niños. As far back as May 2015, BoM noted that the
332 dynamical model averages from the WMO Global Producing Center of Long Range Forecasts
333 (a subset of models in the IRI/CPC plume) were in excess of $+2^{\circ}\text{C}$ for the upcoming fall/winter
334 seasons. ENFEN also noted that Niño 1+2 forecasts created using the North American Multi-
335 model Ensemble (Kirtman et al. 2014) approached the strength of 1997-98.

336 Statistical models largely lagged the growth rate seen in the dynamical models in 2015, and
337 never foresaw the peak amplitude of the event as well as the dynamical models. This disparity
338 is consistent with past ENSO forecasts; in general, the statistical models often lag the dynamical
339 models because they are not configured to take advantage of the most recent changes in the ob-
340 servational evolution (e.g., Barnston et al. 2012). Many statistical models are trained on monthly
341 or seasonal averages, so cannot resolve the short-term changes (e.g. westerly wind bursts) that the
342 dynamical models are initialized with. Thus, the statistical model “success” during 2014 may be
343 due to the fact they were not equipped to react to conditions that the dynamical models saw as
344 important precursors or amplifiers of El Niño growth.

345 Evaluating skill using the temporal anomaly correlation (AC) within a ~ 2 year sliding interval,
346 the dynamical and statistical MME average forecasts were the highest for the most recent event
347 since the IRI/CPC model plume was created in 2002 (see Appendix for details on the forecast
348 verification metrics). Fig. 8 (left column) shows that targets during DJF 2014-FMA 2016 (thick
349 red and blue lines) had the largest AC compared to equivalent length time ranges going back to
350 2002 (grey lines are past windows of 26 consecutive overlapping seasons, each sliding by one
351 season). The thinner red and blue lines correspond to ranges that are strongly associated with the
352 recent period (e.g. NDJ 2013 - JFM 2016). The ACs were in excess of 0.6 going out to lead-8 for
353 both model types, with dynamical models demonstrating slightly more skill for lead-0 to lead-7.
354 The dynamical MME average had an AC greater than 0.9 going out to lead-4, while the statistical
355 MME average only did so going out to lead-2. The AC metric rewards a good fit between the
356 forecast and observational time series during a larger event (relative to a good fit during a smaller
357 event) and, so, the greater AC were partially due to the fact that this event was, by far, the largest
358 in the model record (2002-2016) and was well forecasted.

359 Compared to the AC, the root mean squared error (RMSE) was generally not as skillful relative
360 to past IRI/CPC model forecasts of the Niño-3.4 index (Fig. 8, right column). For the statistical
361 MME, the RMSE was roughly 0.8°C to 1.0°C past lead-4, while they were 0.5°C to 0.8°C for
362 the dynamical MME. For the longest leads, the statistical and dynamical models had amongst
363 the largest errors going back to 2002. Conversely, for the shorter lead times (lead-0 to lead-
364 4), the dynamical MME average had among the smallest errors in the IRI/CPC plume history.
365 Beyond lead-1, the statistical model RMSE remained roughly in the upper quartile of the historical
366 error spread, while improving to the mid-point of the spread for the very shortest leads. Fig. 9
367 indicates that all multi-model averages tend to underestimate the observed values the stronger the
368 event becomes and the longer the lead time (for both El Niño and La Niña). This result may be
369 unsurprising for a large amplitude event, but the low errors (0.2°C to 0.3°C) in the dynamical
370 models at short lead times were rather exceptional.

371 There are other multi-model plumes, such as the North American Multi-Model Ensemble (Kirt-
372 man et al. 2014) and EUROSIP (Palmer et al. 2004), that are increasingly relied upon by forecast-
373 ers who regularly comment on the probability of ENSO events. The advantage of these plumes
374 is that they additionally display the individual ensemble members, which capture the intrinsic
375 “noise” or uncertainty associated with climate forecasts. Probabilistic verification metrics also
376 need to be applied to evaluate whether observations were within the spread of outcomes. It is also
377 worth testing whether the spread of model forecasts reflects the real-world uncertainty because
378 it is generally thought most models are under-dispersive or tend to be overly confident (e.g., Shi
379 et al. 2015).

380 Not only is there uncertainty associated with the models, but there is uncertainty among the ob-
381 servational data used as verification (e.g., Goddard et al. 2009). In general, the prevailing trend is
382 toward development of higher resolution products, so daily OISST was selected herein as the basis

383 for model verification. But, undoubtedly, statistical models, with their generally coarser inputs and
384 outputs, are at an inherent disadvantage when compared against a high-resolution observational
385 dataset. Because statistical models are often built and trained with data from statistical reconstruc-
386 tions (because of the longer records they provide), it may be worthwhile to develop new strategies
387 to increase the resolution of these datasets.

388 **5. Global Anomalies during December-February (DJF)**

389 The strength of El Niño is usually greatest during the Northern Hemisphere winter and its im-
390 pacts generally widespread, with pronounced changes in the Walker circulation across the global
391 tropics and anomalous wave trains that extend into the extratropical latitudes of both hemispheres
392 (Bjerknes 1969; Horel and Wallace 1981). At mid-to-high latitudes, changes to the long-wave pat-
393 tern interacts with synoptic-scale eddies, resulting in the persistence and re-occurrence of storms
394 and other synoptic events over certain regions. As a result, the influence of El Niño is often iden-
395 tified in seasonal averages and not in shorter time averages.

396 During December-February (DJF) 2015-16, above-average 500-hPa geopotential heights dom-
397 inated the tropical latitudes and the mid-latitudes of both hemispheres, with a large anticyclonic
398 anomaly over Siberia during DJF 2015-16 (Fig. 10, top row). Associated with this pattern, strongly
399 above-average temperatures prevailed over most of the globe, with particularly significant positive
400 anomalies over the mid-to-high latitudes of the Northern Hemisphere (Fig. 10, middle row). The
401 most significant regions of increased precipitation were located over the northwestern and south-
402 eastern United States, southern and eastern South America, southeast China, and just south of the
403 equator in eastern Africa (Fig. 10, bottom row). Drier conditions were prominent over northern
404 South America and around Indonesia. So, how well did this observed pattern relate to El Niño?

405 One way to quantify the match is to compute the spatial correlation coefficient between the
406 observed pattern and a typical El Niño pattern. To estimate the latter, detrended DJF climate
407 anomalies are regressed onto standardized and detrended values of the DJF Niño-3.4 index from
408 1979-2014. The regression map is then weighted with the observed DJF 2015-16 Niño-3.4 index
409 value in order to obtain the same units as the observational data (Fig. 10, right column). Thus, the
410 analysis shown here is assuming a linear response to Niño-3.4 SST anomalies and will exclude
411 non-linear relationships. For all three variables in Fig. 10, the spatial correlation coefficients be-
412 tween the observations and the linear ENSO pattern are between 0.3 and 0.5, which means roughly
413 10-25% of the spatial variance was explained by ENSO during DJF 2015-16. While significant,
414 this is not very large, and indicates that there was other variability during the Northern Hemisphere
415 winter that was not well described by this linear estimate of El Niño.

416 The aspects of the circulation that were perhaps most consistent with El Niño were the distinctive
417 wave trains tracing a great circle route across the North and South Pacific Oceans. Anomalous
418 cyclonic flow was observed in the Gulf of Alaska and middle latitudes of the South Pacific Ocean,
419 with anomalous anticyclones poleward and east of the anomalous troughs over Canada and closer
420 to West Antarctica. However, the cyclonic anomaly in the Gulf of Alaska and the anticyclonic
421 anomaly near West Antarctica were shifted northward compared to the typical El Niño response.
422 Over North America, the anomalous warmth projected well onto the El Niño pattern, but the
423 observed anomalies were more intense and widespread than otherwise expected with El Niño.
424 The anticipated pattern of below-average temperatures and heights over the southern tier of the
425 United States did not emerge. Globally, many of the regions that typically experience warmer
426 conditions during El Niño were also above average in 2015-16, and these anomalies were more
427 prominent.

428 Relative to the temperature anomalies, precipitation was more consistent with El Niño during
429 DJF 2015-16. However, there were some notable exceptions from the El Niño pattern, such as
430 the lack of increased precipitation over the southwestern and south-central United States. Like-
431 wise, southernmost Africa was not as dry as one might expect in an El Niño during DJF - though
432 dry conditions over southern Africa were more prominent during ASO through OND 2015 (not
433 shown). In northern Australia, December brought significantly more rainfall than normal, though
434 both January and February were very much below the median — more in line with El Niño ex-
435 pectations. During the 1982-83 and 1997-98 events, devastating rainfall impacted Ecuador and
436 coastal Peru during boreal winter/spring, but this was much weaker in 2015-16. However, the
437 expected drier conditions in the Andean region did prevail in the recent event (see Supp. Fig. 6,
438 which because of low station coverage, provides a comparison with TRMM data).

439 In order to examine longer-term changes, the ~ 35 year linear trend was computed (with its start
440 point at the beginning of the modern satellite era). Interestingly, this simple estimate nearly rivals
441 the ENSO anomalies as a descriptor in the 500-hPa geopotential height anomalies, with a spatial
442 correlation coefficient of 0.37 during DJF 2015-16 (Supp. Fig. 7). Upon inspection, this is found
443 largely due to the Southern Hemisphere trend toward lower heights over Antarctica and higher
444 heights spanning the middle latitudes, which matches well with the observed anomalies. Neither
445 the DJF linear trends in temperature nor precipitation anomalies correlate significantly with the
446 observed pattern (Supp. Fig. 7).

447 To estimate the portion of observed DJF 2015-16 variability that was not related to either the
448 linear trend or linear ENSO, the summed maps are subtracted from the observations (Fig. 11).
449 The resulting so-called “residual” pattern will still include non-linearity in ENSO or any other
450 variability that is not well described by the linear trend or linear ENSO. The stochastic nature of
451 the atmosphere will also result in event-to-event differences. We find that the residual anomalies

452 are highly correlated to the observed pattern with spatial correlation coefficients between 0.5 and
453 0.8. The linear removal clearly does an adequate job removing the elevated heights in the tropics
454 and the typical anomalous wave trains that span the extratropical North and South Pacific during
455 El Niño. What remains are zonal bands of above-average heights encircling the middle latitudes
456 of both hemispheres, with below-average heights located poleward (the only notable exception
457 being the large anticyclonic anomaly near Siberia). Thus, the residual identifies a nearly global,
458 poleward shift in the mid-latitude westerly wind anomalies or jet streams. Accompanying this
459 shift in the Northern Hemisphere, the residual of precipitation is strikingly La Niña-like over the
460 contiguous United States, with rainfall enhanced over the Pacific Northwest and suppressed along
461 the southern tier. Western Europe is also wetter than average, likely due to anomalous westerly
462 flow. Similarly, in the Southern Hemisphere, an anomalous increase in precipitation is evident over
463 southeastern Australia and southern Africa, perhaps due in part to the easterly wind anomalies
464 off the ocean on the equatorward side of the anomalous ridges. The northward shift of the jet
465 (more mid-latitude ridging) and strong anomalous anticyclone near Siberia also overlaps with the
466 strongly above-average temperatures across the Northern Hemisphere extratropics.

467 Despite the fact the observed and residual circulation anomalies have a distinctive annular ap-
468 pearance in the Northern Hemisphere, the DJF 2015/16 Arctic Oscillation (AO) index value was
469 near zero when standardized relative to DJF seasons over 1979-2016. In the Southern Hemisphere,
470 the DJF Antarctic Oscillation (AAO) index was more significant with a positive value of 0.8 stan-
471 dardized units. This outcome was somewhat surprising given El Niño is often associated with
472 negative values of the AAO during November-February (e.g., L'Heureux and Thompson 2006).
473 Instead, increased rainfall over portions of southeastern Australia during DJF 2015-16 appears
474 consistent with the overall positive trend in the AAO (also reflected in Supp. Fig. 7; Hendon et al.
475 2007; Murphy and Timbal 2008; Thomas et al. 2015).

476 Overall, it appears that El Niño coupled with a poleward shift in the jet streams significantly
477 influenced the global climate during December-February 2015-16. It is possible that non-linearity
478 in El Niño (for example, the specific location of the strongest SST anomalies) contributed to the
479 departures from the classically linear anomalies across the globe. Also differences from the linear
480 pattern can be expected to occur simply due to sampling variability, with event-to-event differences
481 naturally arising because of the limited record. It is interesting that a nearly hemispheric structure
482 in the residual circulation was uncovered, which suggests an origin that was not simply isolated to
483 the Pacific sector. The zonal structure may have arisen from random extratropical internal atmo-
484 spheric variability, aided by feedbacks between eddies and the zonal mean flow (e.g., Limpasuvan
485 and Hartmann 2000). Also, positive temperature anomalies throughout the tropical troposphere
486 may have contributed to the poleward shift in the jet (Butler et al. 2010; Lim et al. 2016). A
487 final possibility for the departure from the linear ENSO estimate is the potential influence of sub-
488 seasonal activity across the global tropics (e.g. Kelvin waves, Madden Julian Oscillation), which
489 exerted an influence on tropical rainfall and was aliased into the seasonal averages. We leave it
490 to others to provide a more exhaustive attribution of the possible drivers of the 2015-16 climate
491 anomalies, including exploring other seasons, which can have a greater influence on certain coun-
492 tries (e.g. Australian impacts are largest during the Southern Hemisphere spring).

493 **6. Summary and Future Considerations**

494 Most atmospheric and oceanic indices suggest the 2015-16 El Niño was among the top three
495 strongest El Niño events in the historical record dating back to 1950. While it was not unequiv-
496 cally a record, there were several ways in which this El Niño differed from previous major events
497 in 1982-83 and 1997-98. The west-central Pacific subsurface and surface temperature anomalies
498 were much warmer, while the eastern Pacific was comparatively cooler. As expected during El

499 Niño, the trade winds were weaker, but not as weak during the last half of 2015 as during previous
500 significant events. Related to this, the pressure differences across the tropical Pacific, as measured
501 by the two Southern Oscillation indices, suggest the 2015-16 El Niño had less amplitude relative
502 to the other events. The two OLR indices were both among the top three going back to 1979, but
503 lagged the other two events in the eastern Pacific.

504 In some aspects, the operational model forecasts for the Niño-3.4 index were among the most
505 skillful going back to at least 2002. However, this should not suggest complacency as seen during
506 the borderline El Niño-Neutral situation during 2014-15 when the dynamical models, in partic-
507 ular, largely overestimated the degree of warming. The longest-lead predictions in the dynami-
508 cal, intermediate, and statistical models contain relatively large errors (0.5°C past lead-4), which
509 make predictions of ENSO strength an ongoing challenge. Also, the ensemble average of the
510 multi-model ensemble lagged the initial increases in Niño-3.4 during early 2015, especially for
511 the statistical models, and under-predicted strength beyond the more immediate leads. Statistical
512 models appear to be hampered by their inability to respond to sub-monthly factors that portend
513 ENSO growth, though this may have paradoxically been to their advantage during 2014. While
514 forecast improvements should be sought, an important challenge is to communicate that a portion
515 of forecast uncertainty is irreducible: there will always be error in the initial conditions, boundary
516 forcing, and through the use of imperfect models.

517 Given the historical stature of the 2015-16 El Niño, it is clear that it will be an event that will
518 be vigorously dissected. From an operational perspective, however, there are a couple areas worth
519 examining further. One fundamental challenge is to better understand the influence of trends in the
520 real-time observational data. The WMO recommends that the most recent 30-year base period be
521 used to define anomalies (currently, 1981-2010; Arguez et al. 2012), but it is likely that some part
522 of the ENSO indices is not related purely to ENSO dynamics, but climate change and warming

523 trends. So, how do we best quantify the portion of anomalies related to ENSO versus the portion
524 related to decadal, multi-decadal, or secular variability? And how important is it to diagnose the
525 role of trends when it comes to El Niño monitoring and prediction on a monthly or seasonal basis?
526 For example, what are the consequences of a +2.3°C seasonal Niño-3.4 index value that is revised
527 to +2.1°C after trends are removed? Overall, how substantial is the effect of long-term variability
528 on seasonal ENSO characteristics, dynamics, and predictability?

529 While the scientific understanding of climate change and its consequences has progressed
530 markedly since 1997-98, there are still challenges to quantify and communicate its role on the
531 shorter time scales. While the statistical decomposition in Section 5 is offered as a first estimate,
532 there are certainly other methods to extract the role of various components of the climate system
533 (e.g., Bonfils et al. 2015). Given the tremendous interest from the public to understand the drivers
534 of recent climate anomalies, it remains worthwhile to fine-tune methods and test their applicability
535 to a real-time environment.

536 The 2015-16 event was the first major “24-7 El Niño” coming within a vastly different media
537 setting, with a fast and diverse network (e.g. mobile devices) that did not exist during the last
538 major event of 1997-98. The forecast centers approached this in a variety of ways, using social
539 media, videos and infographics, and blogs (e.g., Climate.gov ENSO Blog , cited 2016) to provide
540 additional information beyond that provided in routine operational assessments, typically issued
541 at bi-weekly to monthly intervals. However, the constant coverage and frequent media updates
542 remained surprising, as ENSO is a slow, seasonally evolving phenomenon that helps set the back-
543 ground flow and increases the chances for certain weather events to re-occur over certain areas,
544 but does not directly cause any weather event.

545 Thus, there was a visible disconnect between the demands of “here and now” coverage and the
546 pace of useful updates that could be provided by the centers on ENSO. For example, while daily or

547 weekly averaged data provides a useful snapshot of tendencies across the tropical Pacific Ocean,
548 it is not currently designed to provide a long, continuous, stable record for historical comparison.
549 Daily and weekly data can also be influenced by a variety of factors outside of ENSO (e.g. tropical
550 cyclones, the Madden-Julian Oscillation, and a number of other intraseasonal phenomena; Hendon
551 and Glick 1997). Yet, despite these caveats, some users relied on these real-time data records to
552 publicize frequent updates on the strength or rank of El Niño. Also, when certain precipitation
553 impacts began to occur, these weather events were sometimes labeled as “El Niño storms” even
554 though El Niño does not directly cause storms, but rather sets the overall background for them.

555 Additionally, there were signs that the forecast for El Niño itself was conflated with the forecasts
556 for associated impacts. At the major national forecast centers, operations related to forecasting
557 ENSO and operations related to creating outlooks of temperature and precipitation may be closely
558 related, but separate endeavors. ENSO is a leading predictor over certain countries and therefore
559 strongly influences the seasonal climate outlook, but it is clearly not the only factor in the models
560 considered by forecasters. The signal-to-noise ratio becomes smaller as one moves away from the
561 tropical Pacific Ocean (e.g., Kumar et al. 2000), and so, for most parts of the world, the confidence
562 in an upcoming ENSO event is likely to be higher than the chance of its related impacts.

563 To clarify some of these service and communication issues, climate services aimed at bridging
564 the provider-user gaps may be helpful. These can range from supporting studies of how users
565 interpret and apply products, to buttressing science communication efforts, such as building easy-
566 to-navigate, clearly described webpages supported by an authoritative social media presence. The
567 role of “learning by doing” also cannot be overstated. With the occurrence of each El Niño event,
568 there are opportunities to learn and apply those lessons to future events. The 2015-16 event was no
569 different in this regard, and will hopefully have provided many users with a greater appreciation

570 of the probabilistic nature of impacts related to El Niño, which needs to be explicitly recognized
571 and factored into their risk analysis and decision-making.

572 *Acknowledgments.* We thank Leigh Zhang (NOAA/CPC) for updating several reanalysis datasets
573 on our behalf. ML, EB, TD, and AB are grateful for support from the NOAA Climate Programs
574 Office (CPO)/Climate.gov for the ENSO Blog. AB also acknowledges NOAA CPO/MAPP grant
575 NA12OAR4310082. KT and KM acknowledge the PP068 program and colleagues at the ENFEN
576 Committee. KT also appreciates the support of the US Embassy in Peru, the Peruvian Embassy in
577 the US, and Min. J. M. Benites.

578 APPENDIX

579 **Verification Metrics**

580 In this paper, the Anomaly Correlation (AC) coefficient is computed as:

$$581 \quad AC = \frac{\overline{x'y'}}{\sigma_x \sigma_y} \quad (A1)$$

582 where x and y are the observational and forecast time series, primes denote anomalies from the
583 time mean, the overbar indicates the average over time, and the sigmas are the standard deviation
584 of x and y. The numerator represents the covariance between x and y.

585 The values associated with the AC lie between -1 and 1 and are dimensionless. Negative values
586 indicate an inverse linear relations between x and y, while positive values indicate a direct linear
587 relations. Values near zero indicate a poor fit between x and y, and values at 1 or -1 reflect a perfect
588 fit or match between the variability in x and y.

589 The Root Mean Squared Error (RMSE) is calculated as:

$$RMSE = \sqrt{\frac{\sum(x-y)^2}{n}} \quad (A2)$$

589 where n is the sample size. The RMSE is the square root of the average of the squares of the
 590 error, or the difference between x and y. Larger RMSE values indicate larger differences either of
 591 the same sign (bias) or of both signs between the observational and forecast time series. Smaller
 592 RMSE indicate smaller differences between the time series.

593 References

594 Arguez, A., I. Durre, S. Applequist, R. S. Vose, M. F. Squires, X. Yin, R. R. H. Jr., and T. W.
 595 Owen, 2012: NOAA's 1981-2010 U.S. climate normals: An overview. *Bull. Amer. Meteor.*
 596 *Soc.*, **93** (11), 1687–1697, doi:10.1175/BAMS-D-11-00197.1.

597 Barnston, A. G., M. Chelliah, and S. B. Goldenberg, 1997: Documentation of a highly ENSO-
 598 related SST region in the equatorial pacific: Research note. *Atmos.-Ocean*, **35** (3), 367–383,
 599 doi:10.1080/07055900.1997.9649597.

600 Barnston, A. G., M. K. Tippett, M. L. L'Heureux, S. Li, and D. G. DeWitt, 2012: Skill of real-time
 601 seasonal ENSO model predictions during 2002-11: Is our capability increasing? *Bull. Amer.*
 602 *Meteor. Soc.*, **93** (5), 631–651, doi:10.1175/BAMS-D-11-00111.1.

603 Bjerknes, J., 1969: Atmospheric teleconnections from the equatorial pacific. *Mon. Wea. Rev.*,
 604 **97** (3), 163–172, doi:10.1175/1520-0493(1969)097<0163:ATFTEP>2.3.CO;2.

605 Bonfils, C. J. W., B. D. Santer, T. J. Phillips, K. Marvel, L. R. Leung, C. Doutriaux, and
 606 A. Capotondi, 2015: Relative contributions of mean-state shifts and ENSO-driven variabil-

607 ity to precipitation changes in a warming climate. *J. Climate*, **28** (24), 9997–10013, doi:
608 10.1175/JCLI-D-15-0341.1.

609 Butler, A. H., D. W. J. Thompson, and R. Heikes, 2010: The steady-state atmospheric circula-
610 tion response to climate change-like thermal forcings in a simple general circulation model. *J.*
611 *Climate*, **23** (13), 3474–3496, doi:10.1175/2010JCLI3228.1.

612 Capotondi, A., and Coauthors, 2015: Understanding ENSO diversity. *Bull. Amer. Meteor. Soc.*,
613 **96** (6), 921–938, doi:10.1175/BAMS-D-13-00117.1.

614 Chen, M., P. Xie, J. E. Janowiak, and P. A. Arkin, 2002: Global land precipitation: A 50-yr
615 monthly analysis based on gauge observations. *J. Hydrometeor.*, **3** (3), 249–266, doi:10.1175/
616 1525-7541(2002)003<0249:GLPAYM>2.0.CO;2.

617 Chiodi, A. M., and D. E. Harrison, 2013: El Niño impacts on seasonal U.S. atmospheric circula-
618 tion, temperature, and precipitation anomalies: The OLR-event perspective. *J. Climate*, **26** (3),
619 822–837, doi:10.1175/JCLI-D-12-00097.1.

620 Climate.gov ENSO Blog, , cited 2016: ENSO Blog. National Oceanic and Atmospheric Admin-
621 istration Climate.gov, [Available online at [https://www.climate.gov/news-features/department/
622 enso-blog](https://www.climate.gov/news-features/department/enso-blog)].

623 Dee, D. P., and Coauthors, 2011: The ERA-interim reanalysis: configuration and performance of
624 the data assimilation system. *Quart. J. Roy. Meteor. Soc.*, **137** (656), 553–597, doi:10.1002/qj.
625 828.

626 DelSole, T., J. Nattala, and M. K. Tippett, 2014: Skill improvement from increased ensemble size
627 and model diversity. *Geophys. Res. Lett.*, **41** (20), 7331–7342, doi:10.1002/2014GL060133,
628 URL <http://dx.doi.org/10.1002/2014GL060133>.

- 629 Fan, Y., and H. van den Dool, 2008: A global monthly land surface air temperature analysis for
630 1948-present. *Journal of Geophysical Research: Atmospheres*, **113** (D1), n/a–n/a, doi:10.1029/
631 2007JD008470, d01103.
- 632 Goddard, L., D. G. DeWitt, and R. W. Reynolds, 2009: Practical implications of uncertainty in
633 observed SSTs. *Geophys. Res. Lett.*, **36** (9), n/a–n/a, doi:10.1029/2009GL037703, 109710.
- 634 Halpert, M. S., and C. F. Ropelewski, 1992: Surface temperature patterns associated with
635 the Southern Oscillation. *J. Climate*, **5** (6), 577–593, doi:10.1175/1520-0442(1992)005<0577:
636 STPAWT>2.0.CO;2.
- 637 Hendon, H. H., and J. Glick, 1997: Intraseasonal air-sea interaction in the Tropical Indian and
638 Pacific oceans. *J. Climate*, **10** (4), 647–661, doi:10.1175/1520-0442(1997)010<0647:IASIIT>2.
639 0.CO;2.
- 640 Hendon, H. H., D. W. J. Thompson, and M. C. Wheeler, 2007: Australian rainfall and surface
641 temperature variations associated with the Southern Hemisphere Annular Mode. *J. Climate*,
642 **20** (11), 2452–2467, doi:10.1175/JCLI4134.1.
- 643 Horel, J. D., and J. M. Wallace, 1981: Planetary-scale atmospheric phenomena associated with
644 the Southern Oscillation. *Mon. Wea. Rev.*, **109** (4), 813–829, doi:10.1175/1520-0493(1981)
645 109<0813:PSAPAW>2.0.CO;2.
- 646 Hu, Z.-Z., A. Kumar, H.-L. Ren, H. Wang, M. LHeureux, and F.-F. Jin, 2013: Weakened in-
647 terannual variability in the tropical Pacific Ocean since 2000. *J. Climate*, **26** (8), 2601–2613,
648 doi:10.1175/JCLI-D-12-00265.1.

649 Huang, B., M. L'Heureux, Z.-Z. Hu, and H.-M. Zhang, 2016: Ranking the strongest ENSO events
650 while incorporating SST uncertainty. *Geophys. Res. Lett.*, n/a–n/a, doi:10.1002/2016GL070888,
651 URL <http://dx.doi.org/10.1002/2016GL070888>, 2016GL070888.

652 Huang, B., W. Wang, C. Liu, V. Banzon, H.-M. Zhang, and J. Lawrimore, 2015a: Bias adjustment
653 of AVHRR SST and its impacts on two SST analyses. *J. Atmos. Oceanic Technol.*, **32** (2), 372–
654 387, doi:10.1175/JTECH-D-14-00121.1.

655 Huang, B., and Coauthors, 2015b: Extended reconstructed sea surface temperature version
656 4 (ERSST.v4). Part I: Upgrades and Intercomparisons. *J. Climate*, **28** (3), 911–930, doi:
657 10.1175/JCLI-D-14-00006.1.

658 Ishii, M., A. Shouji, S. Sugimoto, and T. Matsumoto, 2005: Objective analyses of sea-surface
659 temperature and marine meteorological variables for the 20th century using ICOADS and the
660 Kobe collection. *Int. J. Climatol.*, **25** (7), 865–879, doi:10.1002/joc.1169.

661 Kalnay, E., and Coauthors, 1996: The NCEP/NCAR 40-year reanalysis project. *Bull. Amer. Me-*
662 *teor. Soc.*, **77** (3), 437–471, doi:10.1175/1520-0477(1996)077<0437:TNYRP>2.0.CO;2.

663 Kanamitsu, M., W. Ebisuzaki, J. Woollen, S.-K. Yang, J. J. Hnilo, M. Fiorino, and G. L. Potter,
664 2002: NCEP-DOE AMIP-II Reanalysis (R-2). *Bull. Amer. Meteor. Soc.*, **83** (11), 1631–1643,
665 doi:10.1175/BAMS-83-11-1631.

666 Kirtman, B. P., and Coauthors, 2014: The North American Multimodel Ensemble: Phase-1
667 seasonal-to-interannual prediction; phase-2 toward developing intraseasonal prediction. *Bull.*
668 *Amer. Meteor. Soc.*, **95** (4), 585–601, doi:10.1175/BAMS-D-12-00050.1.

669 Kobayashi, S., and Coauthors, 2015: The JRA-55 Reanalysis: General specifications and basic
670 characteristics. *J. Meteorol. Soc. Jpn. Ser. II*, **93** (1), 5–48, doi:10.2151/jmsj.2015-001.

671 Kumar, A., A. G. Barnston, P. Peng, M. P. Hoerling, and L. Goddard, 2000: Changes in the spread
672 of the variability of the seasonal mean atmospheric states associated with ENSO. *J. Climate*,
673 **13 (17)**, 3139–3151, doi:10.1175/1520-0442(2000)013<3139:CITSOT>2.0.CO;2.

674 Kumar, A., and Z.-Z. Hu, 2014: How variable is the uncertainty in ENSO sea surface temperature
675 prediction? *J. Climate*, **27 (7)**, 2779–2788, doi:10.1175/JCLI-D-13-00576.1.

676 Lee, H.-T., A. Gruber, R. G. Ellingson, and I. Laszlo, 2007: Development of the HIRS outgoing
677 longwave radiation climate dataset. *J. Atmos. Oceanic Technol.*, **24 (12)**, 2029–2047, doi:10.
678 1175/2007JTECHA989.1.

679 Lee, T., and M. J. McPhaden, 2010: Increasing intensity of El Niño in the central-equatorial
680 pacific. *Geophys. Res. Lett.*, **37 (14)**, n/a–n/a, doi:10.1029/2010GL044007, 114603.

681 L’Heureux, M. L., D. C. Collins, and Z.-Z. Hu, 2013: Linear trends in sea surface temperature of
682 the tropical Pacific Ocean and implications for the El Niño-Southern Oscillation. *Climate Dyn.*,
683 **40 (5)**, 1223–1236, doi:10.1007/s00382-012-1331-2.

684 L’Heureux, M. L., and D. W. J. Thompson, 2006: Observed relationships between the El Niño-
685 Southern Oscillation and the extratropical zonal-mean circulation. *J. Climate*, **19 (2)**, 276–287,
686 doi:10.1175/JCLI3617.1.

687 L’Heureux, M. L., M. K. Tippett, and A. G. Barnston, 2015: Characterizing ENSO coupled vari-
688 ability and its impact on North American seasonal precipitation and temperature. *J. Climate*,
689 **28 (10)**, 4231–4245, doi:10.1175/JCLI-D-14-00508.1.

690 Liebmann, B., and C. A. Smith, 1996: Description of a complete (interpolated) outgoing longwave
691 radiation dataset. *Bull. Amer. Meteor. Soc.*, **77 (6)**, 1275–1277.

692 Lim, E.-P., H. H. Hendon, J. M. Arblaster, C. Chung, A. F. Moise, P. Hope, G. Young, and M. Zhao,
693 2016: Interaction of the recent 50 year SST trend and La Niña 2010: Amplification of the
694 Southern Annular Mode and Australian springtime rainfall. *Climate Dyn.*, 1–19, doi:10.1007/
695 s00382-015-2963-9.

696 Limpasuvan, V., and D. L. Hartmann, 2000: Wave-maintained annular modes of climate variabil-
697 ity. *J. Climate*, **13** (24), 4414–4429, doi:10.1175/1520-0442(2000)013<4414:WMAMOC>2.0.
698 CO;2.

699 McPhaden, M. J., 1999: Genesis and evolution of the 1997-98 el niño. *Science*, **283** (5404),
700 950–954, doi:10.1126/science.283.5404.950, [http://science.sciencemag.org/content/283/5404/
701 950.full.pdf](http://science.sciencemag.org/content/283/5404/950.full.pdf).

702 McPhaden, M. J., 2015: Playing hide and seek with El Niño. *Nature Clim. Change*, **5** (9), 791–795,
703 doi:10.1038/nclimate2775.

704 McPhaden, M. J., A. Busalacchi, and D. Anderson, 2010: A TOGA retrospective. *Oceanography*,
705 **23**, URL <http://dx.doi.org/10.5670/oceanog.2010.26>.

706 Murphy, B. F., and B. Timbal, 2008: A review of recent climate variability and climate change in
707 southeastern australia. *Int. J. Climatol.*, **28** (7), 859–879, doi:10.1002/joc.1627.

708 Palmer, T. N., and Coauthors, 2004: Development of a European multimodel ensemble system
709 for seasonal-to-interannual prediction (DEMETER). *Bull. Amer. Meteor. Soc.*, **85** (6), 853–872,
710 doi:10.1175/BAMS-85-6-853.

711 Rayner, N. A., D. E. Parker, E. B. Horton, C. K. Folland, L. V. Alexander, D. P. Rowell, E. C.
712 Kent, and A. Kaplan, 2003: Global analyses of sea surface temperature, sea ice, and night

713 marine air temperature since the late nineteenth century. *J. Geophys. Res. Atmos.*, **108 (D14)**,
714 n/a–n/a, doi:10.1029/2002JD002670, 4407.

715 Reynolds, R. W., N. A. Rayner, T. M. Smith, D. C. Stokes, and W. Wang, 2002: An improved
716 in situ and satellite SST analysis for climate. *J. Climate*, **15 (13)**, 1609–1625, doi:10.1175/
717 1520-0442(2002)015<1609:AIISAS>2.0.CO;2.

718 Reynolds, R. W., T. M. Smith, C. Liu, D. B. Chelton, K. S. Casey, and M. G. Schlax, 2007: Daily
719 high-resolution-blended analyses for sea surface temperature. *J. Climate*, **20 (22)**, 5473–5496,
720 doi:10.1175/2007JCLI1824.1.

721 Rienecker, M. M., and Coauthors, 2011: MERRA: NASA's Modern-Era Retrospective Analysis
722 for research and applications. *J. Climate*, **24 (14)**, 3624–3648, doi:10.1175/JCLI-D-11-00015.1.

723 Roemmich, D., and J. Gilson, 2009: The 2004–2008 mean and annual cycle of temperature, salinity,
724 and steric height in the global ocean from the Argo program. *Progress in Oceanography*, **82 (2)**,
725 81 – 100, doi:http://dx.doi.org/10.1016/j.pocean.2009.03.004, URL http://www.sciencedirect.
726 com/science/article/pii/S0079661109000160.

727 Ropelewski, C. F., and M. S. Halpert, 1987: Global and regional scale precipitation patterns
728 associated with the El Niño/Southern Oscillation. *Mon. Wea. Rev.*, **115 (8)**, 1606–1626, doi:
729 10.1175/1520-0493(1987)115<1606:GARSPP>2.0.CO;2.

730 Saha, S., and Coauthors, 2010: The NCEP Climate Forecast System Reanalysis. *Bull. Amer. Me-*
731 *teor. Soc.*, **91 (8)**, 1015–1057, doi:10.1175/2010BAMS3001.1.

732 Shi, W., N. Schaller, D. MacLeod, T. N. Palmer, and A. Weisheimer, 2015: Impact of hindcast
733 length on estimates of seasonal climate predictability. *Geophys. Res. Lett.*, **42 (5)**, 1554–1559,
734 doi:10.1002/2014GL062829, 2014GL062829.

- 735 Smith, T. M., R. W. Reynolds, T. C. Peterson, and J. Lawrimore, 2008: Improvements to NOAA's
736 historical merged land-ocean surface temperature analysis (1880-2006). *J. Climate*, **21** (10),
737 2283–2296, doi:10.1175/2007JCLI2100.1.
- 738 Takahashi, K., 2004: The atmospheric circulation associated with extreme rainfall events in Piura,
739 Peru, during the 1997–1998 and 2002 El Niño events. *Ann. Geophys.*, **22** (11), 3917–3926.
- 740 Takahashi, K., and B. Dewitte, 2016: Strong and moderate nonlinear El Niño regimes. *Climate*
741 *Dyn.*, **46** (5), 1627–1645, doi:10.1007/s00382-015-2665-3.
- 742 Takahashi, K., A. Montecinos, K. Goubanova, and B. Dewitte, 2011: ENSO regimes: Rein-
743 terpreting the canonical and Modoki El Niño. *Geophys. Res. Lett.*, **38** (10), n/a–n/a, doi:
744 10.1029/2011GL047364, URL <http://dx.doi.org/10.1029/2011GL047364>, 110704.
- 745 Thomas, J. L., D. W. Waugh, and A. Gnanadesikan, 2015: Southern Hemisphere extratropical
746 circulation: Recent trends and natural variability. *Geophys. Res. Lett.*, **42** (13), 5508–5515, doi:
747 10.1002/2015GL064521, 2015GL064521.
- 748 Vecchi, G. A., and D. E. Harrison, 2006: The termination of the 1997?98 El Niño. Part I: Mecha-
749 nisms of oceanic change. *J. Climate*, **19** (12), 2633–2646, doi:10.1175/JCLI3776.1.
- 750 Vecchi, G. A., A. T. Wittenberg, and A. Rosati, 2006: Reassessing the role of stochastic forcing
751 in the 1997-1998 El Niño. *Geophys. Res. Lett.*, **33** (1), n/a–n/a, doi:10.1029/2005GL024738,
752 101706.

753 **LIST OF TABLES**

754 **Table 1.** Current ENSO Systems for Australia, Peru, and the United States 35

TABLE 1: Current ENSO Systems for Australia, Peru, and the United States

Australian Bureau of Meteorology

El Niño / La Niña Watch: The chance of an El Niño developing in the coming season has increased. When these criteria have been met in the past, El Niño / Niña has developed around 50% of the time. The criteria are:

- (1) ENSO phase is currently neutral or La Niña / El Niño is declining
- (2) EITHER: of the closest ten analogue years (based on the Southern Oscillation Index (SOI)), four or more have shown El Niño / La Niña characteristics OR significant sub-surface warming (El Niño) / cooling (La Niña) has been observed in the western or central equatorial Pacific Ocean
- (3) One-third or more of surveyed climate models show sea surface temperature (SST) at least 0.8°C above average (El Niño) / below average (La Niña) in the Niño-3 or Niño-3.4 regions by late winter or spring

El Niño / La Niña Alert: The chance of an El Niño / La Niña developing in the coming season has increased. When these criteria have been met in the past, El Niño / La Niña has developed around 70% of the time. Any three of the following criteria are met:

- (1) A clear warming (El Niño) / cooling (La Niña) trend has been observed in the Niño-3 or Niño-3.4 regions during the past three to six months
- (2) Trade winds have been weaker (El Niño) / stronger (La Niña) than average in the western or central equatorial Pacific Ocean during any two of the last three months
- (3) The two-month average SOI is -7 or lower (El Niño) / +7 or higher (La Niña)
- (4) A majority of surveyed climate models show SSTs at least 0.8°C above average (El Niño) / below average (La Niña) in the Niño-3 or Niño-3.4 regions by the late winter or spring

El Niño / La Niña: An El Niño / La Niña has been declared and is underway. Any three of the following criteria are met:

- (1) Temperatures in the Niño-3 or Niño-3.4 regions are 0.8°C warmer (El Niño) / cooler (La Niña) than average
- (2) Trade winds have been weaker (El Niño) / stronger (La Niña) than average in the western or central equatorial Pacific Ocean during any three of the last four months.
- (3) The three-month average SOI is -7 or lower (El Niño) / +7 or higher (La Niña)
- (4) A majority of surveyed climate models show SSTs remaining at least 0.8°C above average (El Niño) / below average (La Niña) in the Niño-3 or Niño-3.4 regions of the Pacific until the end of the year

Updated as part of the ENSO Wrap-Up: <http://www.bom.gov.au/climate/enso/>

ENFEN Committee (Comité encargado del Estudio Nacional del Fenómeno El Niño, Peru)

ENFEN monitors and predicts El Niño/La Niña in two regions:

“Coastal” El Niño/La Niña: When the Índice Costero El Niño (ICEN; 3-month running-mean Niño 1+2 SST index, <http://www.met.igp.gob.pe/datos/icen.txt>) is above/below 0.4°C/-1.0°C for three or more consecutive months. The overall strength of the event is determined by the three largest ICEN values in the event, according to pre-established thresholds. In the Northern Hemisphere winter/spring, warming can produce heavy rain over the arid coast.

“Central Pacific” El Niño/La Niña: Based on the Niño 3.4 SST index using a threshold of +/-0.5°C. This impacts the Peruvian Andes and Amazon through teleconnections.

The following are the Alert system states for the coastal El Niño/La Niña:

Coastal El Niño/La Niña Watch: There is a higher expectation that El Niño/La Niña will occur than not.

Coastal El Niño/La Niña Alert: The El Niño/La Niña is believed to have started based on observed ocean-atmosphere conditions and/or if the ICEN) qualifies.

Inactive: Neutral conditions are present or El Niño/La Niña are expected to end.

Updated as part of the ENFEN Official Statements: http://www.imarpe.pe/imarpe/lista.php?id_seccion=I01660200000000000000

National Oceanic and Atmospheric Administration (NOAA) Climate Prediction Center, United States

El Niño/La Niña Watch: When oceanic and atmospheric conditions across the tropical Pacific are favorable for the onset of El Niño/La Niña within the next 6 months

El Niño/La Niña Advisory: When El Niño/La Niña conditions are present as measured by three criteria:

El Niño Advisory:

- (1) 1-month Niño-3.4 SST index value that is at or in excess of +0.5°C
- (2) Atmospheric conditions are consistent with El Niño (i.e. weaker low-level trade winds, enhanced convection over the central or eastern Pacific Ocean)
- (3) The expectation that El Niño will persist as measured by at least 5 overlapping seasonal (3-month average) Niño-3.4 SST index values at or in excess of +0.5°C.

La Niña Advisory:

- (1) 1-month Niño-3.4 SST index value that is at or less than -0.5°C
- (2) Atmospheric conditions are consistent with La Niña (i.e. stronger low-level trade winds, suppressed convection over the central Pacific Ocean)
- (3) The expectation that La Niña will persist as measured by at least 5 overlapping seasonal (3-month average) Niño-3.4 SST index values at or less than -0.5°C.

Final El Niño/La Niña Advisory: When El Niño/La Niña has ended.

Not Active (NA): The ENSO Alert System is not active.

Updated as part of the ENSO Diagnostics Discussion: http://www.cpc.ncep.noaa.gov/products/analysis_monitoring/enso_advisory/index.shtml

755 **LIST OF FIGURES**

- 756 **Fig. 1.** Evolution of seasonal (3-month) averaged values of the Niño-3.4 SST index (top left panel),
 757 Niño-4 SST index (top right panel), Niño-3 SST index (bottom left panel), and Niño-1+2
 758 SST index (bottom right panel) during 2015-16 (red), 1997-98 (blue), 1982-83 (green), and
 759 1972-73 (purple). The Niño-3.4 region is 5°N-5°S, 170°W-120°W, the Niño-4 region is
 760 5°N-5°S, 150°W-160°E, the Niño-3 region is 5°N-5°S, 150°W-90°W, and the Niño-1+2
 761 region is 0°-10°S, 90°W-80°W (regions displayed in Fig. 6). Thin lines correspond to the
 762 ERSSTv3b, ERSSTv4, COBE, and HadISST datasets and the thicker lines is the average of
 763 all datasets. Departures are formed by removing monthly means during 1981-2010. 38
- 764 **Fig. 2.** Longitude-Time (Hovmoller) diagram of weekly SST anomalies across the equatorial Pa-
 765 cific Ocean (5°S-5°N) from 120°E to 80°W during 2015-16 (left panel), 1997-98 (middle
 766 panel), and 1982-83 (right panel). Departures are formed by removing the first four har-
 767 monics of interpolated daily data during 1981-2010. Data are based on weekly OISSTv2.
 768 39
- 769 **Fig. 3.** Longitude-Time (Hovmoller) diagram of 5-day running averages of the 20°C isotherm depth
 770 (in meters) across the equatorial Pacific (2°S-2°N) from 135°E to 75°W during 2015-16
 771 (left panel) and 1997-98 (right panel). Data is based on the Tropical Atmosphere Ocean
 772 (TAO) moored buoys from 11 transects and Argo floats near 85°W. A 5-day running mean
 773 was applied and spatial interpolation is based on Python contourf. The data was processed
 774 by the Instituto Geofisico del Peru using the 1981-2010 climatology obtained from NCEP
 775 GODAS. 40
- 776 **Fig. 4.** Longitude-Time (Hovmoller) diagram of daily 10-meter zonal wind anomalies across the
 777 equatorial Pacific Ocean (5°S-5°N) from 120°E to 80°W during 2015-16 (left panel) and
 778 1997-98 (middle panel), and the difference between 2015-16 and 1997-98 (right panel).
 779 Departures are formed by removing the first four harmonics of interpolated daily data during
 780 1981-2010. Data are based on ERA-Interim. 41
- 781 **Fig. 5.** Evolution of seasonal (3-month) averaged values of the traditional Tahiti-Darwin station
 782 based Southern Oscillation Index (dashed lines) and Equatorial Southern Oscillation Index
 783 (EQSOI; solid lines) (top panel), Central Pacific Outgoing Longwave Radiation (OLR) index
 784 (middle panel), and Eastern Pacific OLR index (bottom panel) during 2015-16 (red), 1997-
 785 98 (blue), and 1982-83 (green). The EQSOI is based on the difference between the region
 786 from 5°N-5°S, 80°W-130°W and 5°N-5°S, 90°E-140°E. CP OLR is based on the region
 787 from 170°E-140°W, 5°S-5°N and the EP OLR region is 160°W-110°W, 5°S-5°N. Thin solid
 788 lines in the top panel correspond to the NCEP CFSR (Saha et al. 2010), NCEP/NCAR
 789 Reanalysis I (Kalnay et al. 1996), NCEP/DOE Reanalysis II (Kanamitsu et al. 2002), ERA-
 790 Interim (Dee et al. 2011), JRA-55 (Kobayashi et al. 2015), NASA MERRA1, and MERRA2
 791 (Rienecker et al. 2011). Thin solid lines in the middle and bottom panels are from AVHRR
 792 and the HIRS v2r2 and v2r7. The thick solid line in all panels is the average of individual
 793 datasets. All indices are standardized using monthly means and standard deviations during
 794 1981-2010. 42
- 795 **Fig. 6.** SST anomaly reconstruction based on the weighted regression map of the Niño-3.4 index
 796 (top left panels) and the observed SST anomalies during 2015-16 (top right panels) for sea-
 797 sonal averages during June-August (JJA), November-January (NDJ), and February-April
 798 (FMA). The spatial correlation between the reconstruction and observations is on the ordi-
 799 nate and the seasonal average Niño-3.4 index value is on the abscissa (bottom panels). Each
 800 dot represents a single year between 1982-2016. The red dots indicate the 2015-16 El Niño,
 801 two other strong El Niños in 1997-98 and 1982-83, and the 2009-10 El Niño, which is the El

802	Niño prior to the 2015-16 event. The top left panel displays the Niño-4 region (blue), Niño-	
803	3.4 region (thin red), Niño-3 region (green), and Niño-1+2 region (aqua). Departures are	
804	formed by removing monthly means during 1981-2010. Data are based on weekly OISSTv2.	43
805	Fig. 7. Predictions of the Niño-3.4 index for overlapping, seasonal target periods from December	
806	2013 - February 2014 (DJF) to February-April 2016 (FMA) for the dynamical models (top	
807	panel) and statistical models (bottom panel) drawn from the IRI/CPC plume. Grey lines	
808	show every individual model forecast and the red and blue lines show the dynamical and	
809	statistical multi-model averages, respectively. The thick black line shows the observational	
810	data based on seasonal averages of daily OISST data.	44
811	Fig. 8. The anomaly correlation (left column) and root mean squared error (right column) between	
812	the observations and multi-model averages of the dynamical (top row) and statistical (bottom	
813	row) forecasts of the Niño-3.4 index. The thick blue and red lines show the skill for targets	
814	during December 2013 - February 2014 (DJF) to February-April 2016 (FMA). The grey	
815	lines are the skill of past windows of 26 consecutive overlapping seasons, each sliding by one	
816	season, with thin blue and red lines showing windows that overlap with the DJF 2013/14-	
817	FMA 2016 period. Forecast data are verified against seasonal averages of daily OISST data.	
818		45
819	Fig. 9. Scatterplots of observed Niño-3.4 index values (plotted on the abscissa) against Lead-0 (top	
820	row), Lead-4 (middle row), Lead-8 (bottom row) forecasts based on the dynamical (left	
821	column) and statistical (right column) multi-model averages (plotted on the ordinate) for all	
822	seasonal (3-month) averages dating back to the beginning of the model plume in February	
823	2002. The color shading shows the year of the target season, and the numeral highlights the	
824	location of the November-December-January (NDJ) target season and year (displaying last	
825	two digits between 2002-2015). The r-value in the top left corner is the correlation between	
826	the observations and forecasts made between February 2002 and April 2016. Forecast data	
827	are verified against seasonal averages of daily OISST data.	46
828	Fig. 10. December 2015-February 2016 anomalies of 500-hPa geopotential height and winds (top	
829	row), surface temperature (middle row), and precipitation (bottom row). The left column	
830	shows the observational data, while the right column shows the reconstruction for 2015/16	
831	(weighted regression map of the Niño-3.4 index). The r-values show the spatial correla-	
832	tion coefficient between the observational and the reconstructed anomalies (cosine weighted	
833	by latitude). Geopotential height and wind data is from the NCEP/NCAR Reanalysis, the	
834	temperature is from the gridded GHCN+CAMS dataset, and precipitation data is from the	
835	gridded Precipitation Reconstruction Dataset (PREC) dataset. Departures are formed by	
836	removing monthly means during 1981-2010.	47
837	Fig. 11. As in Figure 10, except showing the residual anomalies formed from subtracting the trend	
838	plus ENSO reconstruction from the observational data. The r-values show the spatial correla-	
839	tion coefficient between the observational and the residual anomalies.	48

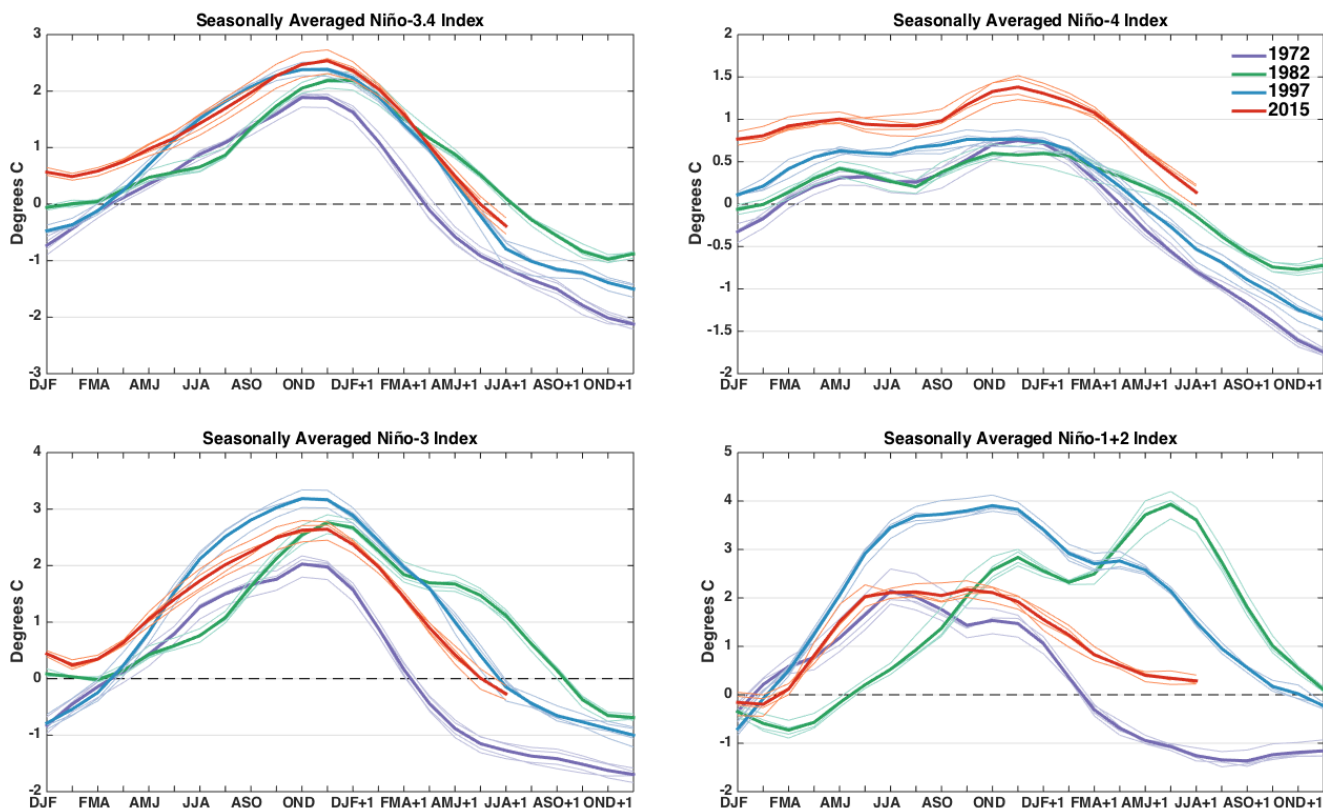


FIG. 1: Evolution of seasonal (3-month) averaged values of the Niño-3.4 SST index (top left panel), Niño-4 SST index (top right panel), Niño-3 SST index (bottom left panel), and Niño-1+2 SST index (bottom right panel) during 2015-16 (red), 1997-98 (blue), 1982-83 (green), and 1972-73 (purple). The Niño-3.4 region is 5°N - 5°S , 170°W - 120°W , the Niño-4 region is 5°N - 5°S , 150°W - 160°E , the Niño-3 region is 5°N - 5°S , 150°W - 90°W , and the Niño-1+2 region is 0° - 10°S , 90°W - 80°W (regions displayed in Fig. 6). Thin lines correspond to the ERSSTv3b, ERSSTv4, COBE, and HadISST datasets and the thicker lines is the average of all datasets. Departures are formed by removing monthly means during 1981-2010.

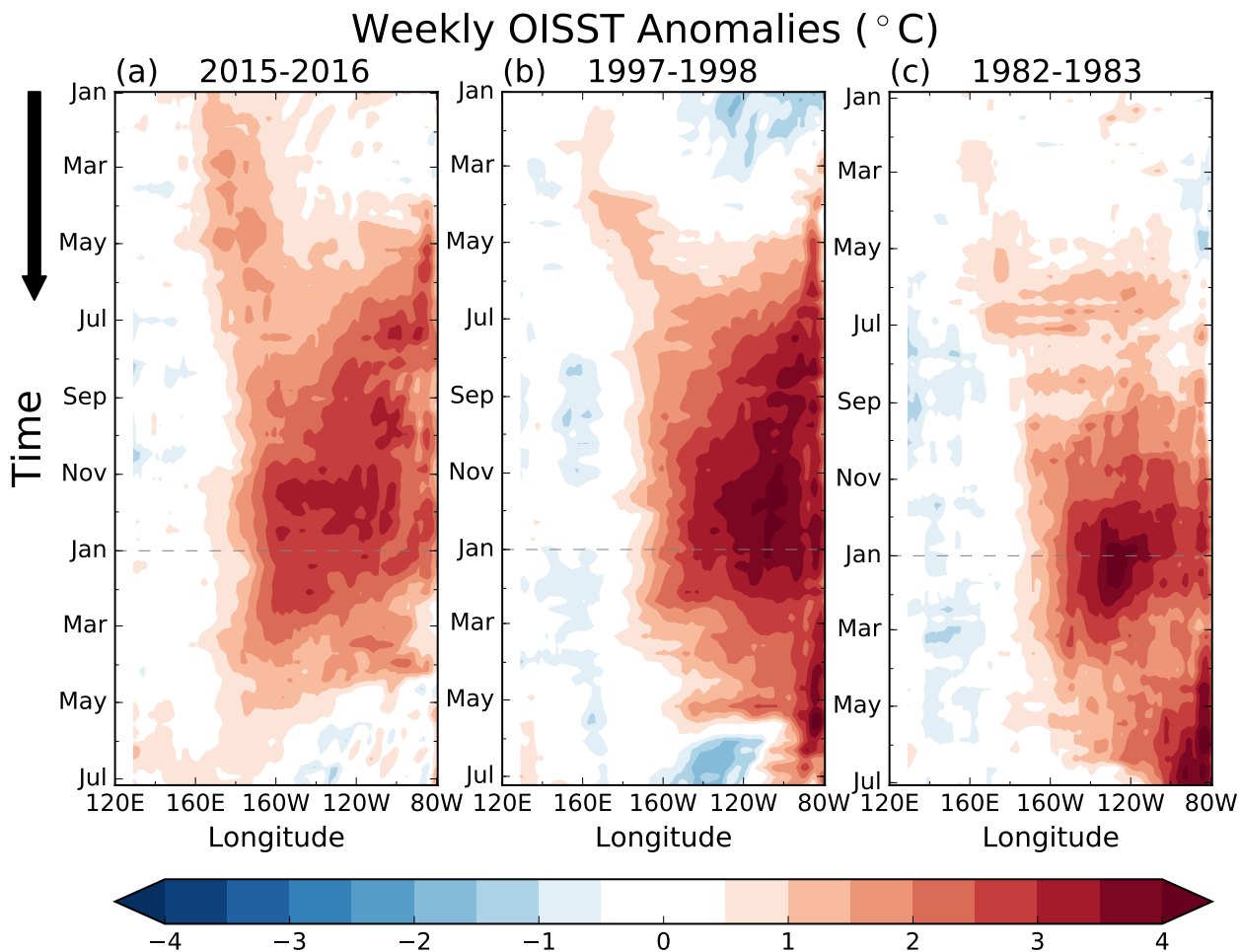


FIG. 2: Longitude-Time (Hovmoller) diagram of weekly SST anomalies across the equatorial Pacific Ocean (5°S - 5°N) from 120°E to 80°W during 2015-16 (left panel), 1997-98 (middle panel), and 1982-83 (right panel). Departures are formed by removing the first four harmonics of interpolated daily data during 1981-2010. Data are based on weekly OISSTv2.

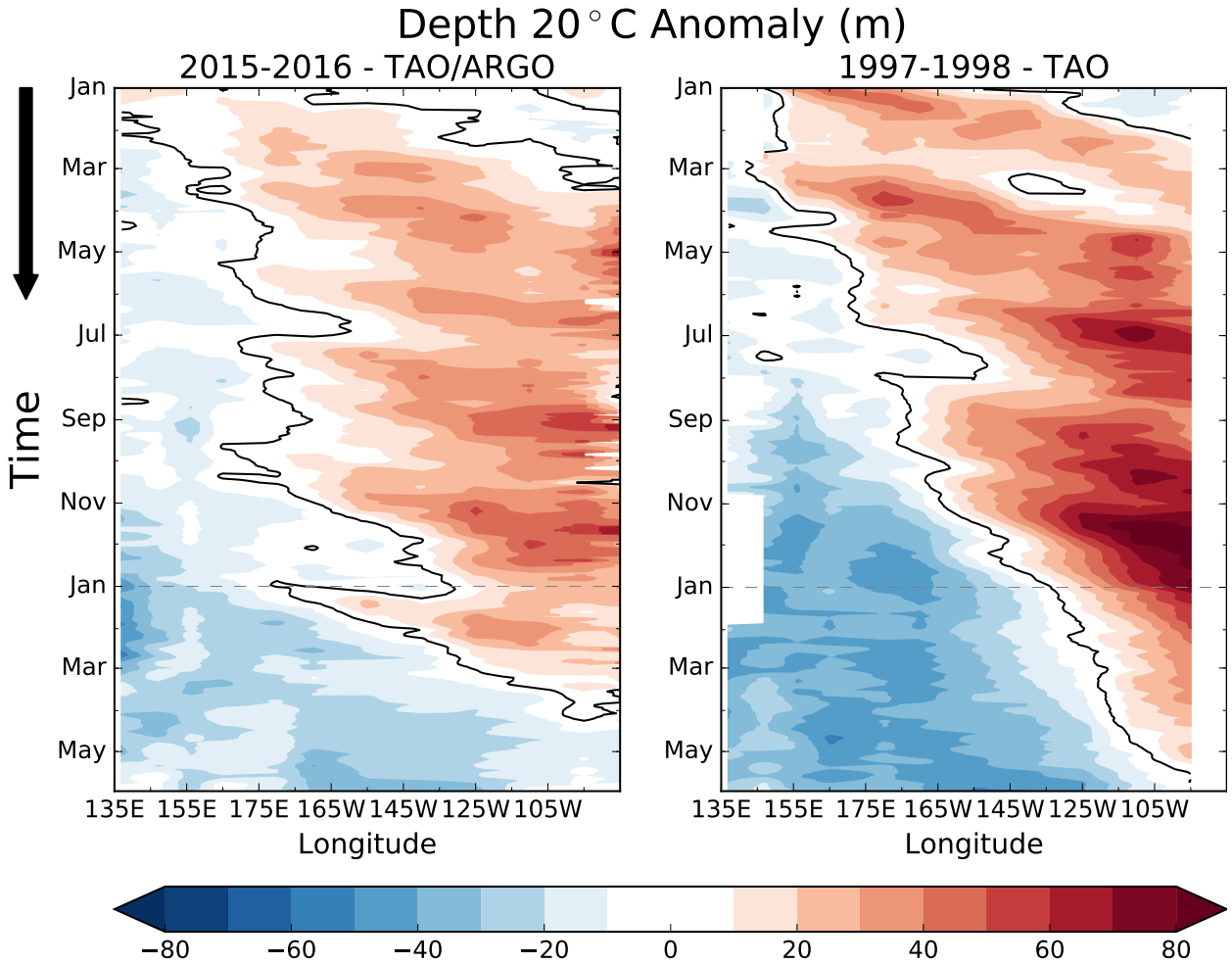


FIG. 3: Longitude-Time (Hovmoller) diagram of 5-day running averages of the 20°C isotherm depth (in meters) across the equatorial Pacific (2°S-2°N) from 135°E to 75°W during 2015-16 (left panel) and 1997-98 (right panel). Data is based on the Tropical Atmosphere Ocean (TAO) moored buoys from 11 transects and Argo floats near 85°W. A 5-day running mean was applied and spatial interpolation is based on Python contourf. The data was processed by the Instituto Geofisico del Peru using the 1981-2010 climatology obtained from NCEP GODAS.

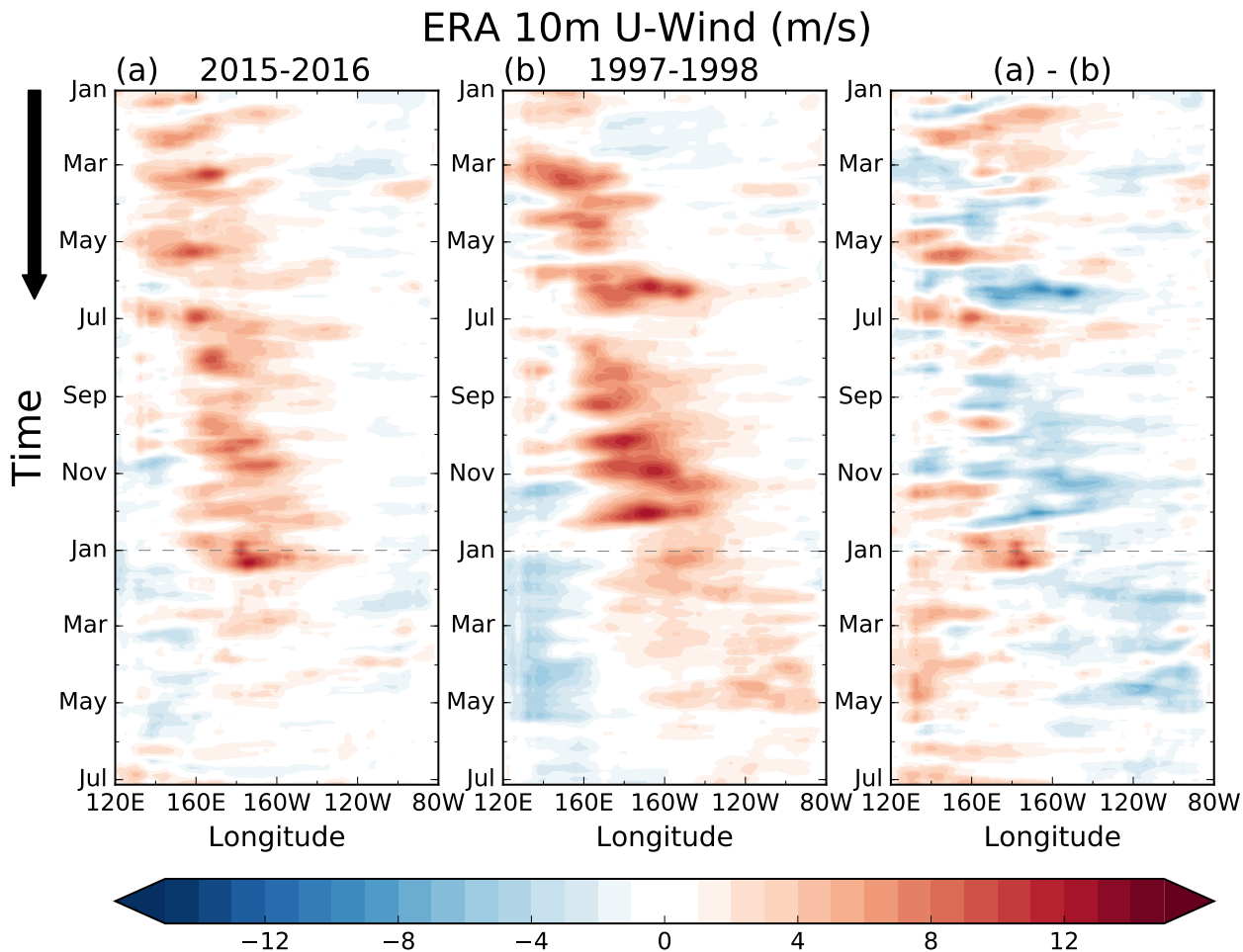


FIG. 4: Longitude-Time (Hovmoller) diagram of daily 10-meter zonal wind anomalies across the equatorial Pacific Ocean (5°S - 5°N) from 120°E to 80°W during 2015-16 (left panel) and 1997-98 (middle panel), and the difference between 2015-16 and 1997-98 (right panel). Departures are formed by removing the first four harmonics of interpolated daily data during 1981-2010. Data are based on ERA-Interim.

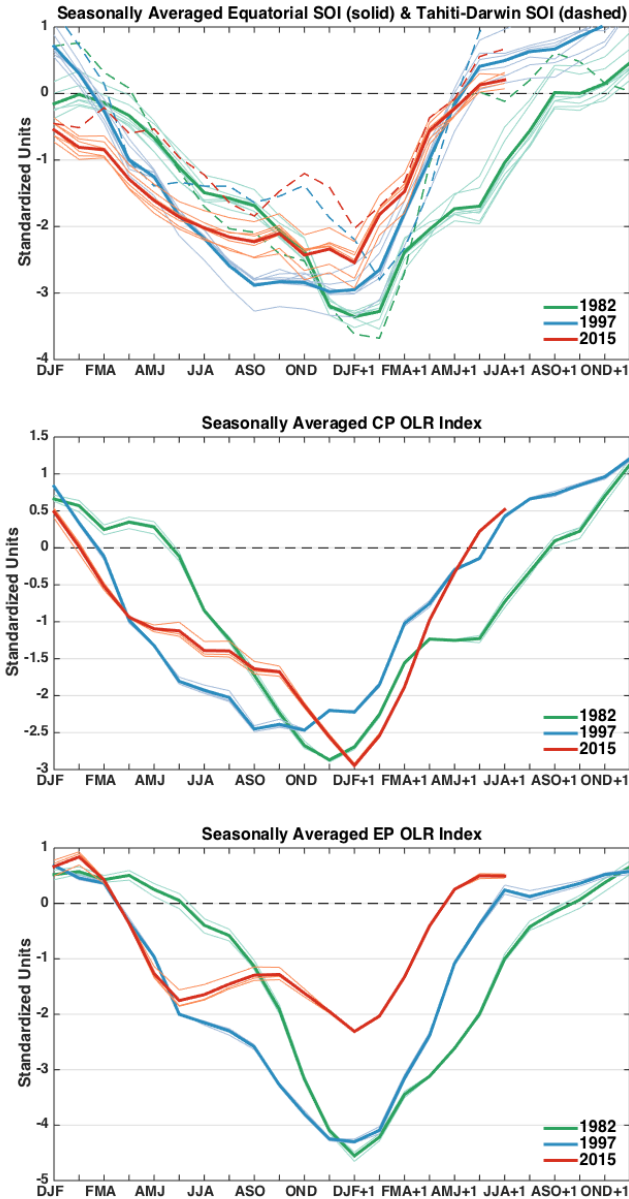


FIG. 5: Evolution of seasonal (3-month) averaged values of the traditional Tahiti-Darwin station based Southern Oscillation Index (dashed lines) and Equatorial Southern Oscillation Index (EQ-SOI; solid lines) (top panel), Central Pacific Outgoing Longwave Radiation (OLR) index (middle panel), and Eastern Pacific OLR index (bottom panel) during 2015-16 (red), 1997-98 (blue), and 1982-83 (green). The EQSOI is based on the difference between the region from 5°N - 5°S , 80°W - 130°W and 5°N - 5°S , 90°E - 140°E . CP OLR is based on the region from 170°E - 140°W , 5°S - 5°N and the EP OLR region is 160°W - 110°W , 5°S - 5°N . Thin solid lines in the top panel correspond to the NCEP CFSR (Saha et al. 2010), NCEP/NCAR Reanalysis I (Kalnay et al. 1996), NCEP/DOE Reanalysis II (Kanamitsu et al. 2002), ERA-Interim (Dee et al. 2011), JRA-55 (Kobayashi et al. 2015), NASA MERRA1, and MERRA2 (Rienecker et al. 2011). Thin solid lines in the middle and bottom panels are from AVHRR and the HIRS v2r2 and v2r7. The thick solid line in all panels is the average of individual datasets. All indices are standardized using monthly means and standard deviations during 1981-2010.

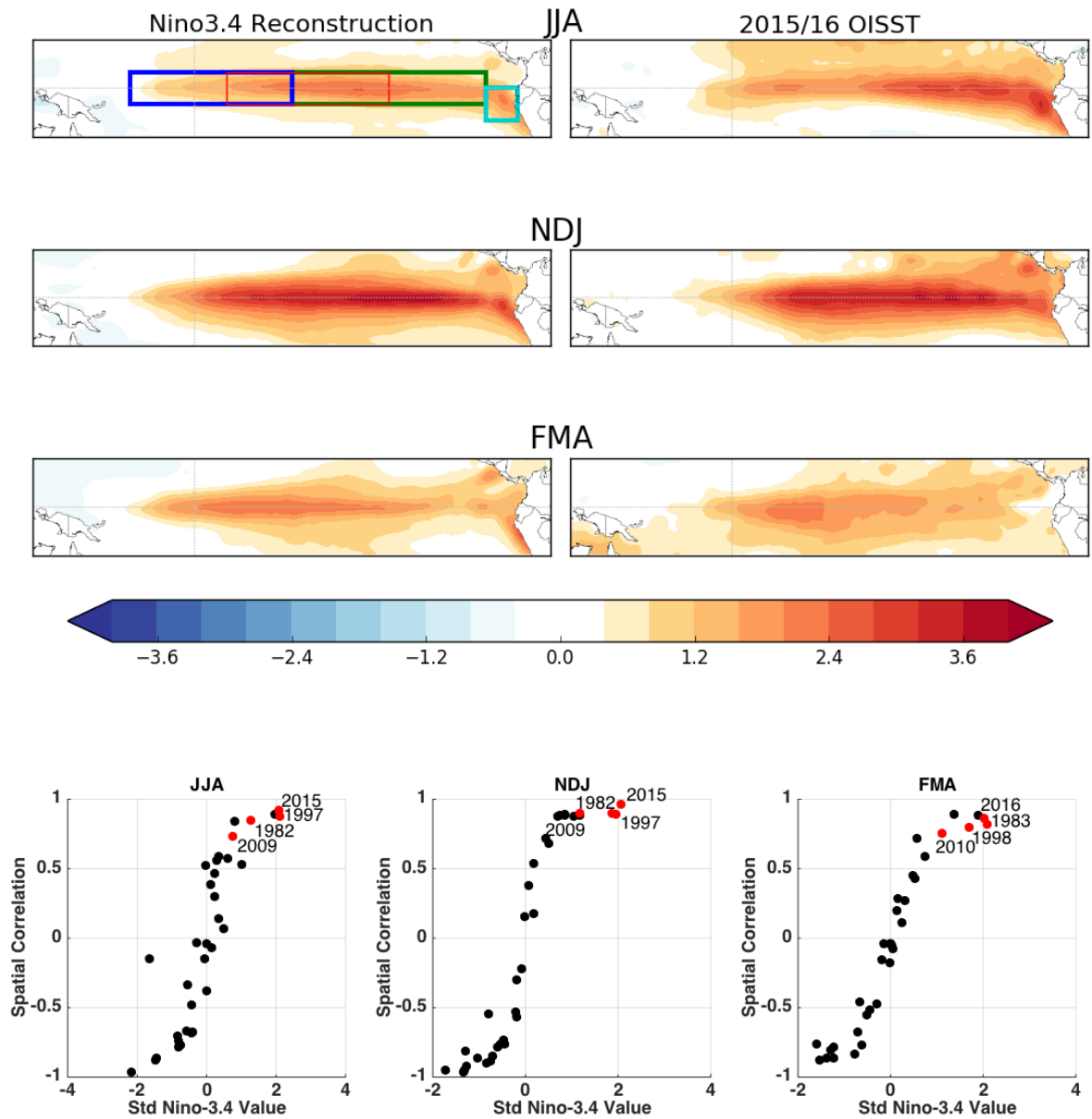


FIG. 6: SST anomaly reconstruction based on the weighted regression map of the Niño-3.4 index (top left panels) and the observed SST anomalies during 2015-16 (top right panels) for seasonal averages during June-August (JJA), November-January (NDJ), and February-April (FMA). The spatial correlation between the reconstruction and observations is on the ordinate and the seasonal average Niño-3.4 index value is on the abscissa (bottom panels). Each dot represents a single year between 1982-2016. The red dots indicate the 2015-16 El Niño, two other strong El Niños in 1997-98 and 1982-83, and the 2009-10 El Niño, which is the El Niño prior to the 2015-16 event. The top left panel displays the Niño-4 region (blue), Niño-3.4 region (thin red), Niño-3 region (green), and Niño-1+2 region (aqua). Departures are formed by removing monthly means during 1981-2010. Data are based on weekly OISSTv2.

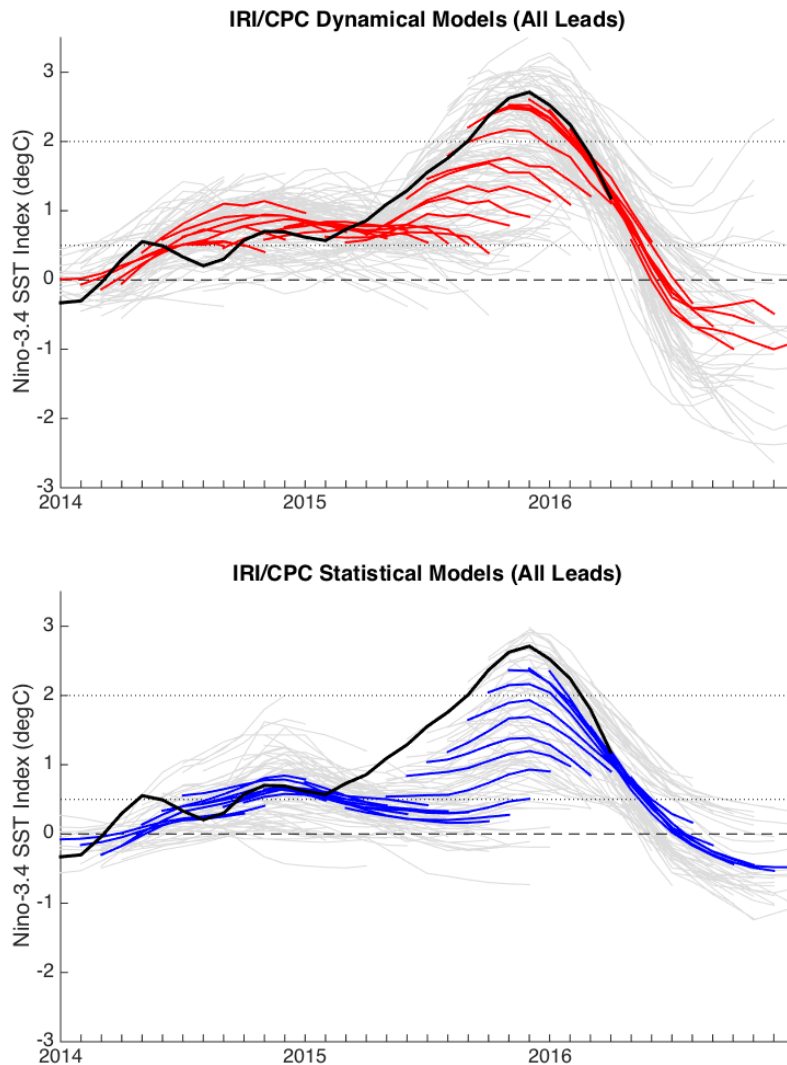


FIG. 7: Predictions of the Niño-3.4 index for overlapping, seasonal target periods from December 2013 - February 2014 (DJF) to February-April 2016 (FMA) for the dynamical models (top panel) and statistical models (bottom panel) drawn from the IRI/CPC plume. Grey lines show every individual model forecast and the red and blue lines show the dynamical and statistical multi-model averages, respectively. The thick black line shows the observational data based on seasonal averages of daily OISST data.

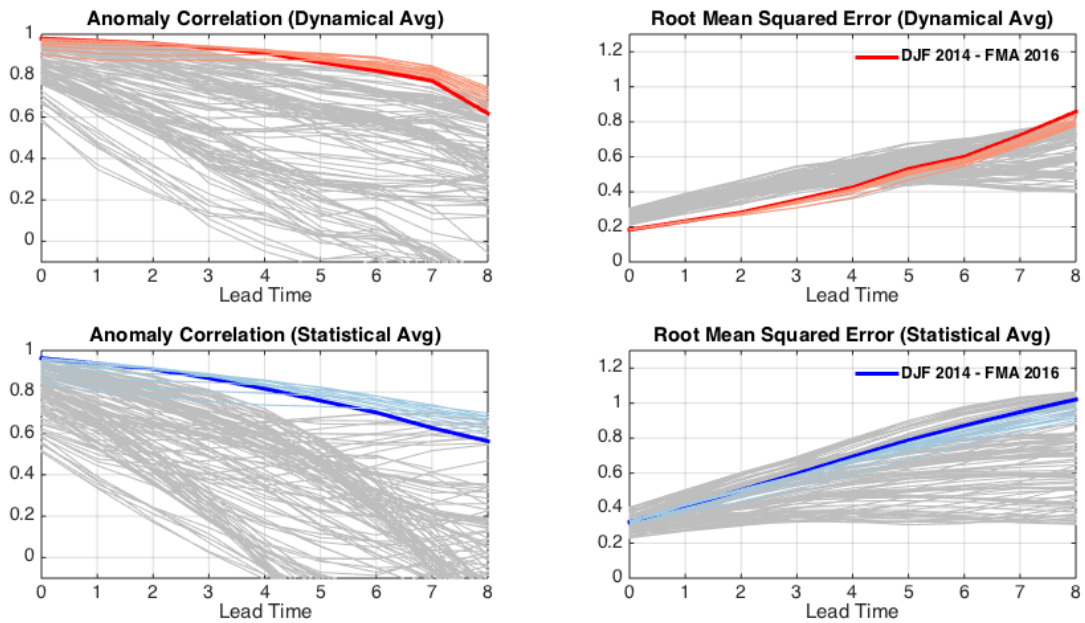


FIG. 8: The anomaly correlation (left column) and root mean squared error (right column) between the observations and multi-model averages of the dynamical (top row) and statistical (bottom row) forecasts of the Niño-3.4 index. The thick blue and red lines show the skill for targets during December 2013 - February 2014 (DJF) to February-April 2016 (FMA). The grey lines are the skill of past windows of 26 consecutive overlapping seasons, each sliding by one season, with thin blue and red lines showing windows that overlap with the DJF 2013/14-FMA 2016 period. Forecast data are verified against seasonal averages of daily OISST data.

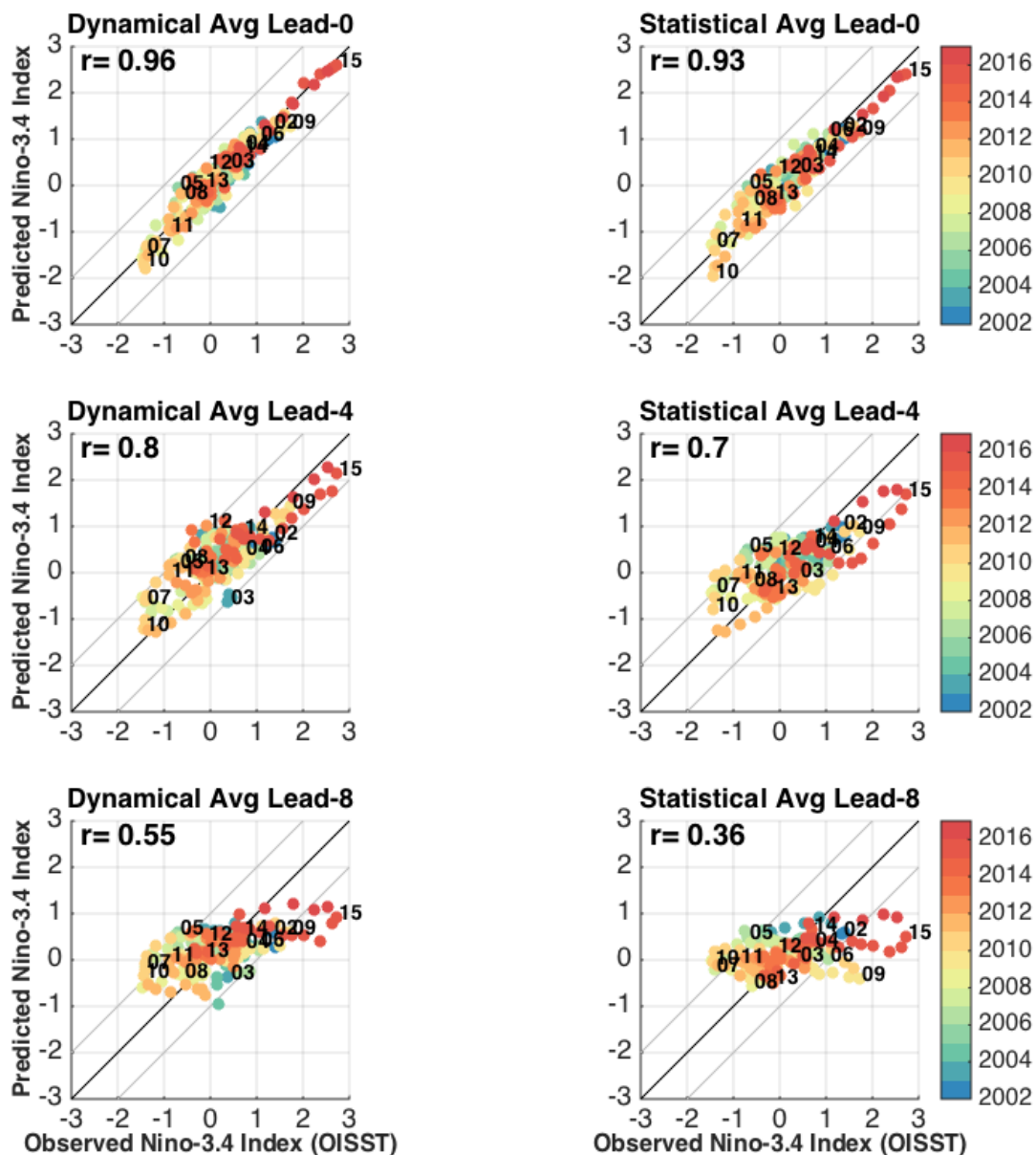


FIG. 9: Scatterplots of observed Niño-3.4 index values (plotted on the abscissa) against Lead-0 (top row), Lead-4 (middle row), Lead-8 (bottom row) forecasts based on the dynamical (left column) and statistical (right column) multi-model averages (plotted on the ordinate) for all seasonal (3-month) averages dating back to the beginning of the model plume in February 2002. The color shading shows the year of the target season, and the numeral highlights the location of the November-December-January (NDJ) target season and year (displaying last two digits between 2002-2015). The r-value in the top left corner is the correlation between the observations and forecasts made between February 2002 and April 2016. Forecast data are verified against seasonal averages of daily OISST data.

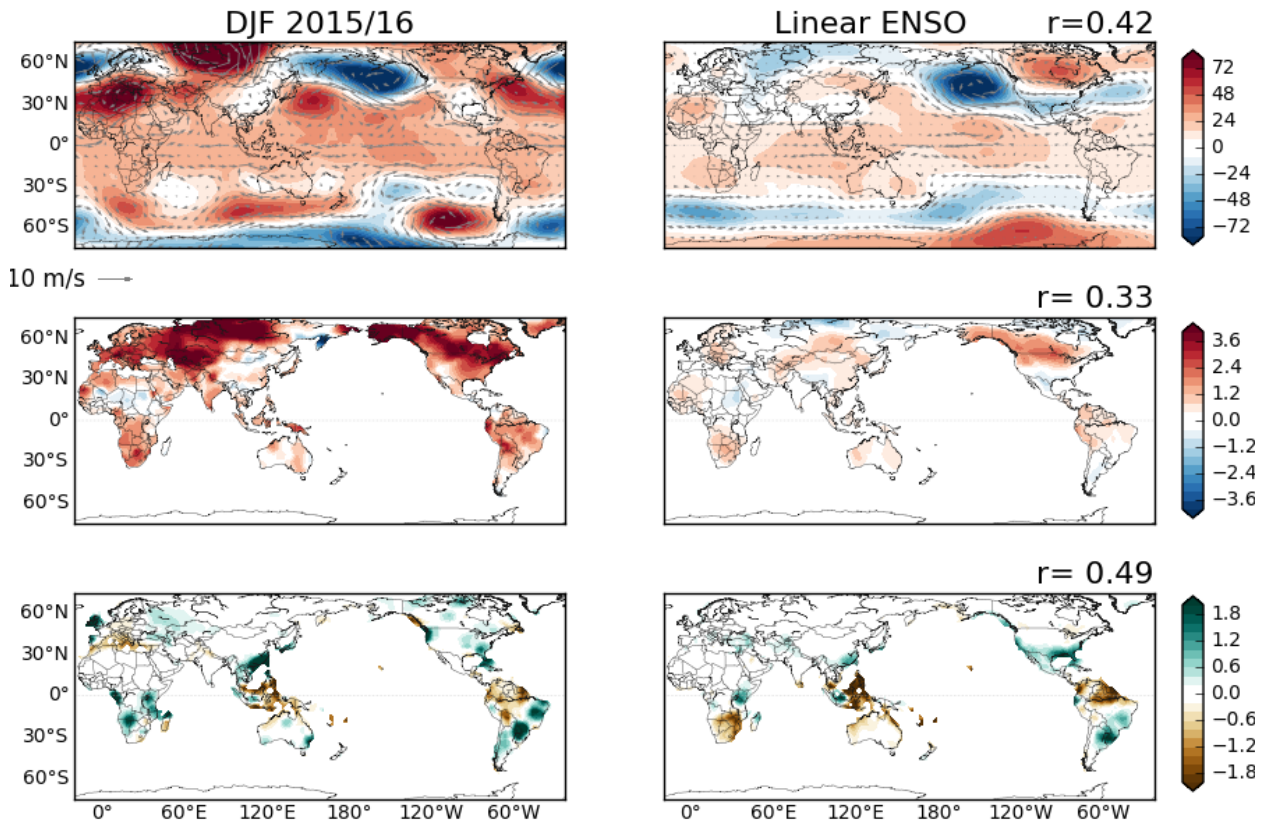


FIG. 10: December 2015-February 2016 anomalies of 500-hPa geopotential height and winds (top row), surface temperature (middle row), and precipitation (bottom row). The left column shows the observational data, while the right column shows the reconstruction for 2015/16 (weighted regression map of the Niño-3.4 index). The r -values show the spatial correlation coefficient between the observational and the reconstructed anomalies (cosine weighted by latitude). Geopotential height and wind data is from the NCEP/NCAR Reanalysis, the temperature is from the gridded GHCN+CAMS dataset, and precipitation data is from the gridded Precipitation Reconstruction Dataset (PREC) dataset. Departures are formed by removing monthly means during 1981-2010.

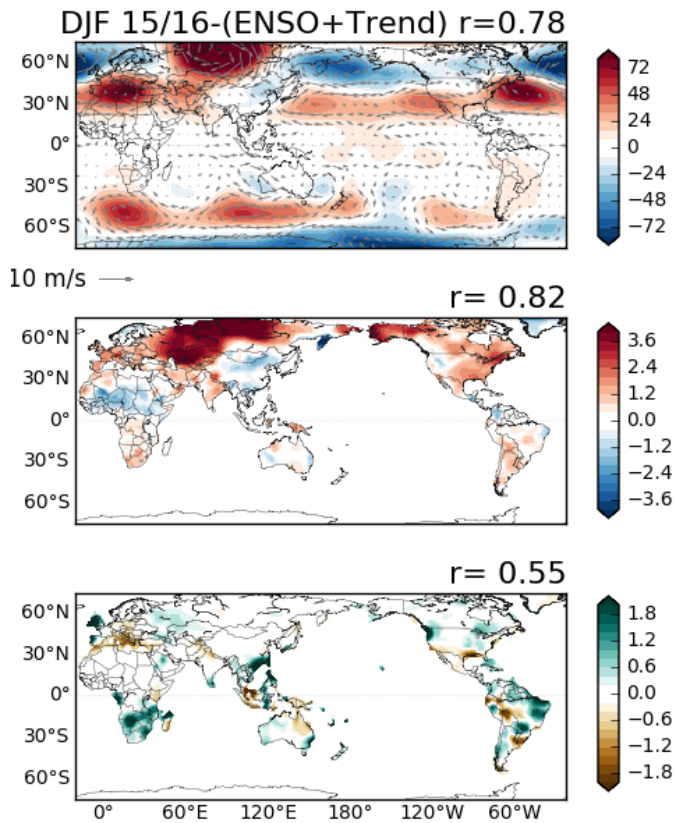


FIG. 11: As in Figure 10, except showing the residual anomalies formed from subtracting the trend plus ENSO reconstruction from the observational data. The r -values show the spatial correlation coefficient between the observational and the residual anomalies.